OSLO METROPOLITAN UNIVERSITY
STORBYUNIVERSITETET

Department of Civil Engineering and Energy Technology
Institutt for Bygg- og energiteknikk
Energi og miljø i bygg
Postal address: Postboks 4 St. Olavs plass, 0130 Oslo
Visiting address: Pilestredet 35, Oslo

MASTER'S THESIS

TITLE OF THE MASTER'S THESIS	DATE
Understanding airborne respiratory droplets in relation to different ventilation strategies	2022-5-25
	NR. OF PAGES/APPENDICES
	54/11

AUTHOR	SUPERVISOR
Ole Martinius Harket Norbeck	Arnab Chaudhuri

WRITTEN/PERFORMED IN COLLABORATION WITH	CONTACT PERSON
Convergent Science GmbH, Austria	Suresh Kumar Nambully

ABSTRACT

To investigate the potential of airborne transmission of human respiratory events, this study presents a realistic approach to human breathing, coughing, and speaking in a small double office, involving both static human beings and human motion. We evaluate the dispersion of droplets in various scenarios utilizing both mixing ventilation (MV) and displacement ventilation (DV) with varied air changes per hour (ACH) using a finite volume method (FVM) based 3D multiphase flow solver. A user defined function (UDF) that establishes a cut-of radius of 2.5 μm to stop additional evaporation is implemented to investigate the transient behavior of the respiratory particles inside the domain.

3 KEY WORDS
Computational fluid dynamics
AMR
Airborne transmission

Abstract

Viral transmissions from human beings has emerged into a hot topic over the past several years as the world has faced severe repercussions on societies, economies and health following COVID-19. Understanding the dynamics of respiratory events such as coughing, breathing and speaking remains to be fully understood, especially in the mode of airborne transmission.

This study presents a realistic approach to human breathing, coughing and speaking in a small double office considering scenarios involving static human beings as well as human motion. Utilizing a finite volume method based 3D multiphase flow solver, we assess the dispersion of droplets in various scenarios using both mixing ventilation (MV) and displacement ventilation (DV) with different air changes per hour (ACH). To analyze the transient behaviour of the respiratory particles within the domain a user defined function (UDF) is implemented that defines a cut-of radius of 2.5 μm to cease further evaporation.

In comparison to MV, we detect a clear tendency that DV inhibits the dispersion of respiratory particles at both high and low ACH. In terms of particle removal, the current conditions make it difficult to determine which ventilation method is better. To reach a conclusion on the efficiency, more research is required.

Sammendrag

Virale overføringer fra mennesker har blitt et mye omdiskutert tema i løpet av de siste årene, ettersom verdens samfunn, økonomi og helse har møtt alvorlige konsekvenser som følge av COVID-19. Forståelsen av dynamikken til respirasjonshendelser som hosting, pusting og snakking er fortsatt ufullstendig, spesielt i forhold til luftbåren smitte.

Denne studien presenterer en realistisk tilnærming til menneskelig pusting, hosting og snakking i et lite dobbeltkontor, hvor en rekke scenarier som involverer stillesittende mennesker, i tillegg til mennesker i bevegelse blir undersøkt. Ved å bruke et "finite volume method" (FVM)-basert 3D simuleringsprogram for å løse den komplekse dynamikken, vurderer vi spredningen av dråper ved å undersøke både omrøringsventilasjon (MV) og fortrengningsventilasjon (DV) med forskjellige luftmengder (ACH). For å analysere strømningsmønsteret til partiklene i rommet, implementeres en brukerdefinert funksjon (UDF) som definerer en "cut-off" radius på 2,5 μm for å stoppe ytterligere fordampning av partiklene.

Sammenlignet med MV, oppdaget vi en klar tendens til at DV hindrer spredningen av partikler ved både høye og lave luftmengder. Når det gjelder fjerning av partikler, fører den etablerte metoden til at det er vanskelig å avgjøre hvilken ventilasjonsmetode som fungerer best. For å komme til en endelig konklusjon om effektiviteten til ventilasjonsprinsippene er det nødvendig med ytterligere forskning på området.

Preface

This master's thesis represents the end of the degree "Energi og miljø i bygg - sivilingeniør" at Oslo Metropolitan university. The work has been done during the spring of 2022.

I will initiate this by acknowledging my supervisor, Arnab Chaudhuri, for excellent guidance and support throughout this semester. Fluid dynamics has been a difficult subject to comprehend, but your knowledge and experience in the field has created a fun and effective learning environment. You have been available day and night to help out with what ever was needed, which has been more than appreciated. Thank you for an instructive and rewarding semester.

Secondly, i would like to thank Oda Martine Sundsdal for the collaboration on the initial verification of the model, the SIMS 2022 paper and endless support throughout the semester. Working alongside you during these months has been a big motivation and very much appreciated.

Further acknowledgements are due to Suresh Kumar Nambully at Convergent Science GmbH, for invaluable assistance on understanding the CONVERGE 3.0 solver and clarification of uncertainties related to the model setup. I would not have been able to do this without your help.

Last but not least, a big thanks to my family and friends for constant encouragement and support the past five years on Oslomet.

Contents

List of Figures

List of Tables

1 Introduction

The outbreak of SARS-CoV-2 (COVID-19) has made the world more aware of the serious repercussions following a large scale pandemic. Globally, approximately 496 million confirmed cases and over 6 million deaths have been reported as of April 10, 2022 [1]. Virus outbreaks and pandemics have been a part of the world as we know it as far as we can trace back in time and it is evident that a new pandemic will govern our way of living in the future as well. The research on this topic has increased since the outbreak of COVID-19 and the importance of gaining a solid understanding of infection paths and particle/droplet trajectories is detrimental for the future, seeing how the current pandemic has influenced the global societies, economies and health. As a result, it's clear that even more research should be focused on infection-prevention and methods to reduce the spread of infections, both on a personal level as well as an environmental level such as public indoor spaces, due to the fact that most people spend 90% of their day indoors [2].

The main route of infection is through respiratory fluids carrying the contagious virus. Exposure occurs either by inhalation of very fine droplets and aerosols, through droplets and particles depositing on exposed mucous membranes in the mouth, nose, and eyes, and by being in contact with surfaces containing infectious virus [3]. Due to a lack of evidence, there was a disagreement in the early days of the outbreak about whether COVID-19 spreads through airborne particles. This has eventually been confirmed to be one of the primary modes of transmission, which explains situations like super-spreading events [4]. As a result, the world has experienced high infection rates leading to the widespread pandemic [5]. Respiratory fluids are emitted into the environment during breathing, speaking and coughing etc, potentially carrying infectious virus. The distribution of droplets varies across a wide spectrum of sizes ranging from small droplet nuclei and aerosol particles at sub-micrometer level, usually characterized as smaller than 5 μm in diameter and particles larger than 5 μm, characterized as droplets [6]. The larger droplets tends to be dominated by gravity, creating a ballistic trajectory settling to the ground within a short period of time before they evaporate, for distances usually up to 2m in indoor spaces [7]. Small droplets and aerosols evaporate faster than they settle and turns into droplet nuclei floating in the room for minutes and in some cases several hours. Droplet nuclei is defined by WHO as "the residue of dried respiratory aerosols that results from evaporation of droplets exhaled into the atmosphere" [6]. Meaning the nuclei can be characterized as mass-less and will be dominated by buoyancy forces and the local airflow.

The emphasis on social distancing and especially the technical designs in public buildings must not the taken lightly as the ventilation system plays an important role of creating a healthy indoor environment by supplying fresh air into the room and extracting the pollutant air through the outlet. Ventilation design has to be adapted to each building specifically depending on its use case. Common ventilation design used in offices, schools and residential buildings with mechanical ventilation are either mixing ventilation or displacement ventilation. A mixing design is where fresh air is supplied near the roof at high velocities and extracted from outlets located at ceiling level, creating a well mixed space. Displacement ventilation supplies fresh air at low speeds near the lower part of the wall or from the floor, most commonly used in larger public indoor areas. The purpose of such design is to take advantage of the buoyancy forces to accelerate the air throughout the entire floor space lifting it above

the occupant zone due to local heat sources such as technical equipment and humans, and extracting it through the outlets in the ceiling or upper part of the wall.

Understanding the role of human breathing, talking and coughing in relation to spread of infection is critical when making mitigation strategies for an indoor environment. To comprehend viral transmission and devise preventive measures, careful considerations of local airflow, air change per hour, droplet mechanics and relative humidity must be made.

1.1   Literature review

Experimental and numerical approaches are needed for a thorough understanding of the mechanism of viral transmission as they complement each other to a high degree. Experiments are the bedrock of numerical studies, allowing for high-quality investigation into scenarios that would otherwise be difficult or unattainable. Computational fluid dynamics (CFD) is a numerical method that is extremely useful and widely utilized by scientists for this purpose, especially post COVID-19. Cough, sneeze, breathing, talking as well as singing and its relation to droplet transmission has been investigated incorporating different aspects of the complex topic, such as droplet size distribution, spatial distribution, droplet dispersion, evaporation etc. The risk of virus transmission from such respiratory events has relevance in all sorts of public areas, creating numerous scenarios and areas in need of investigation. Confined spaces is amongst the most relevant topics, including elevators, classrooms, conference rooms, offices and gyms [8]. Computational multiphase fluid solver combined with an Eulerian-Lagrangian approach is amongst the most popular ways of resolving the complex flow physics with CFD. Dbouk and Drikakis [7] employed such approach to better understand the mechanisms of a human cough and its relation to airborne transmission and social distancing. More precisely, the transport, dispersion and evaporation of coughed saliva particles. A mild human cough at a room temperature of 20°C and a relative humidity of 50% was found to travel considerable distances depending on the local wind speed. With wind speeds between 4 km/h to 15 km/h, droplets could travel up to 6 m. In two similar separate reports [9, 10], they look into the transmission of respiratory droplets through and around a face mask filter for cough instances, as well as the impact of air ventilation systems on airborne virus transmission in a confined space (elevator setup). Their results show that masks are effective for preventing the spread of droplets, however it does not provide complete protection, as many droplets will still spread around the cover of the mask. Penetration dynamics of airborne droplet transmission, fluid dynamics leakage around the filter and the reduction of efficiency during cough cycles are shown to be important areas that needs more attention and is not considered in todays employed criterion for assessing face masks. New criterion for more accurate assessment of masks is proposed. Further, they contribute to broader understanding on the topic of airborne virus transmission in confined spaces. Through investigating three different ventilation setups in an elevator and a fourth setup with air purifier, they show that the placement of inlets and outlets has significant influence on flow circulation and dispersion of droplets and highlights the importance of engineering designs of such spaces. A similar study by Patrick Paulsen [11] revisited a human cough instance in an elevator setup focusing on saliva droplet dynamics in relation to relative humidity. His study reveals that adaptive mesh refinement (AMR) is beneficial for solving complex multiphase flows. At a RH of 40% he shows that 35% of a single cough instance with a mass of 7.7 μg will evaporate.

A study conducted related to airborne spread of influenza from 2015 looked into the uncertainties concerning possible influence of airborne virus transmission [12]. They looked at the amount of virus that was expelled by patients in aerosol particles while coughing. A total of 64 participants were asked to cough six times into a cough aerosol collection system, where 17 of the participants tested positive for influenza A. The results show that viable influenza A virus was detected in the aerosol particles from 7 of the 17 test subjects with sizes ranging from 0.3 μm to 8 μm. Another report from 2018 provides compelling evidence that humans generate infectious aerosols and that it's not only limited to respiratory events of higher magnitude, like cough and sneeze [13].

Following these findings, experts from all over the world disputed whether COVID-19 also might be transmitted through the air. Even though evidence was present, little effort was put towards mitigation of airborne transmission by the World Health Organization (WHO). In June of 2020 Morawska and Milton appealed to the medical community and relevant international and national bodies to recognize the potential for airborne spread of COVID-19 and advocated for the use of preventive measures to mitigate the infection route [14]. With signatures and studies from credible scientists, they demonstrate that viruses are released during exhalation without any doubt and that micro-droplets at sizes of 5 μm will remain airborne for a significant amount of time and travel beyond 1-2 m. Highlighting the fact that conventional measures such as hand washing and maintaining social distance are insufficient. Morawska and Cao [15] further emphasized the concern in their paper from July 2020, by reviewing existing literature summarizing the seriousness of airborne transmission.

Moreover, several studies has dealt with the issue of airborne transmission of small droplets and aerosols using CFD with an emphasis on the importance of ventilation [16, 17]. Vuorinen et al. utilized physics-based modeling using both RANS and LES to investigate the physical processes related to aerosol dispersion in air in a supermarket, mainly from a cough [18]. Alongside this, a Monte-Carlo simulation was implemented to understand a transmission scenario via inhalation of aerosols. Their findings state that typical cough- or speech generated droplets of sizes up to 20 μm can stay airborne for 20 min - 1 hr depending on the rate of evaporation. They also showed that size of droplets between 50 μm - 100 μm can remain in the air for 3 min - 20 s. To assess the risk of inhaling potentially virus-containing particles, Shao [19] used in situ measurements and CFD simulations to estimate the expelled particles from normal pulmonary breathing and their transport under elevator, small classroom, and supermarket settings. They report that inappropriate design of ventilation systems can limit the efficiency of particle removal, create local hot spots and enhance deposition of particles to surfaces. Through experiments using Schlieren imaging and digital inline holography they characterized particle formation, size distribution, and concentration and show that breathing patterns are comparable among individuals. The measured particles sizes were below 5 μm.

While airborne transmission is found by several studies to be a fact, the measures of mitigation of such particles still remains a challenge. As stated by several studies mentioned, the design of ventilation systems has several important factors to it that needs to be addressed, including ACH, filters, placement of inlet/outlet and re-circulation of air. A review paper by Lipinski et al. [20] investigated current ventilation systems in schools and offices with the purpose of determining whether additional development is required, and which actions are required to limit the risk of infection posed

by pandemics. Based on their findings, mixing ventilation leads to disadvantages as they increase the range of infectious particles within the room and the range of sizes of particle that can sustainably remain airborne. On the other hand, displacement ventilation is a preferred option because of the nature of the design. Fresh air is inserted at low velocities near the floor, ensuring slow movement of contaminated air directly to the exhaust in the ceiling while reducing the concentration of airborne particles. Further, they highlight that recirculating ventilation strategies must be avoided to ensure that contaminated air is not reused potentially carrying infectious virus. Mariam et al.[21] used CFD simulations to study spatial transmission of COVID-19 vectors in a typical office room as well as airborne particle dispersion due to coughing, sneezing, normal and loud talking. Their focus was on different placement of the inlet and outlet combined with different ACH. They show that talking can lead to a high concentration of particles persisting for long times regardless of less particles being exhaled compared to i.e a cough. The study suggests "air curtains" as an appropriate approach, and highlights that increasing the ACH not necessarily is a good solution. Another study recently published [22] investigated the spread of droplets during coughing, talking and normal breathing in a conference room setting occupied by ten people, using numerical analyses. They looked into different scenarios with and without air conditioning, and with and without masks applying a realistic approach to respiratory patterns as well as a realistic meeting scenario. The mass flow rate from the exhaled air was calculated based on a developed mathematical expression in accordance with literature. The findings reveal that normal breathing patterns, affected by people's thermal plumes and buoyancy forces, send small droplets upwards towards the ceiling. They also stress the necessity of proper ventilation to eliminate polluted air.

A common agreement amongst the above mention studies is that the design of ventilation strategies are critical in reducing the risk of particle encounters. Despite the fact that several new studies on the subject have been published during the pandemic, a lack of understanding is still present. Studies incorporating a more realistic scenario and combinations of human breathing, talking and coughing combined with ventilation designs in public building are not abundant. A highly relevant scenario that receives little attention is the effect of human motion in combination with respiratory instances in public settings. Li et al. [23] studied several scenarios involving a coughing person on an escalator with the intention of analyzing the dispersion of the droplets using numerical simulations with varying slope and speed. Their findings states that the slope significantly alters the vertical concentration of droplets in the passengers wake. A descending escalator creates higher suspension height and a bigger spread of the droplets and suggests that the social distancing guidelines may be inadequate and that more research are needed. In a separate study by Li et al. [24] they studied the role of motion on the dispersion of coughed droplets. Using numerical CFD simulations, they considered a person walking 1.5 m/s in a confined space that are varied in size. For all the studies cases, similar results are found regarding the vertical height of the droplets for distances larger than 2m behind the walking person. The height is below waist level, creating risks for children walking behind a coughing person.

1.2 Objective

In the present study, we present a realistic approach to human breathing, coughing and speaking in a small double office considering scenarios involving static human beings as well as human motion. This work aims to assess the droplet dispersion in different scenarios using both mixing ventilation and displacement ventilation with different ACH, and contribute by assessing the effectiveness of such ventilation strategies in reducing the spread of particles from a human respiratory event. The Eulerian dispersion medium is considered as a multicomponent mixture consisting of O_2, N_2 and H_2O and the discrete phase considers the droplets as H_2O, computed using the Lagrangian method. The unsteady flow dynamics is solved using an advanced three dimensional multiphase flow solver with adaptive mesh refinement, CONVERGE 3.0. A user defined function (UDF) has been integrated specifying that droplets smaller than or equal to a radius of 2.5 μm will cease to evaporate, making it possible to track the movement of the smallest droplets over time to recreate a realistic scenario. The thesis is organized as follows. Section one includes introduction and review of relevant studies on the topic. In section two we present the methods, including theoretical background of the computation, model and problem setup and methods concerning simulations and incorporation of UDF, followed by results, discussion and conclusions in section 3 and 4.

2 Methods

In this section the methods and relevant theory governing the numerical analysis will be presented. This includes the explanation of fluid mechanics governing equations, ventilation strategies, a description of the model and problem setup, as well as essential post-processing and simulation approaches.

2.1 Theoretical background

Droplet transport from a respiratory event is governed by complex physics that needs to be fully understood for the creation of a realistic model. This section will present the governing equations and relevant dynamics that determines the fate of the particles emitted from a respiratory event.

2.1.1 Governing equations

Fluid flow dynamics are governed by the non-linear coupled transport equations of Navier-Stokes, which describes the conservation of mass, momentum and energy of newtonian fluids [25]. This applies to all kinds of viscous fluid flow scenarios and is the base of the physical model. The behaviour of fluid is described in terms of properties such as velocity, pressure, density and temperature, and their space and time derivatives [26]. The continuity equation is given in equation 1 and solves the conservation of mass of a unsteady, thee-dimensional point in a compressible fluid.

$$\frac{\partial \rho}{\partial t} + \nabla(\rho \mathbf{u}) = 0 \tag{1}$$

The first term of equation 1 describes the rate of change in time of the density and the second term is the convective term, and describes the net flow of mass out of the element across its boundaries. ρ is the density, u is the velocity and t is time.

The momentum and energy equations states the changes of properties either in a fluid particle or for a collection of fluid elements making up a fixed region in space. If the properties in a fluid particle is considered it can be referred to as the Lagrangian approach and if fixed fluid elements is considered it can be referred to as the Eulerian approach. The momentum equation is a statement of Newton's second law and can be defined as the rate of increase of momentum of fluid particle equals the sum of forces on fluid particle [26]. The equation in general form is shown in equation 2.

$$\rho \frac{D\mathbf{u}}{Dt} = -\nabla p + \nabla \cdot \tau + \rho \mathbf{g} \tag{2}$$

Where ρ is the density, g is the gravity, τ is the stress and t is time.

The third and final equation one of the governing equations is the conservation of energy. This is defined as rate of increase of energy of fluid particle equals net rate of heat added to fluid particle plus the net rate of work done on fluid particle. The equation has its origin from the first law of thermodynamics and is shown in equation 3 below.

$$\frac{\partial(\rho i)}{\partial t} + \nabla(\rho i \mathbf{u}) = -p\nabla \mathbf{u} + \nabla(k\nabla T) + \phi + S_i \tag{3}$$

i is internal energy, k is the thermal conductivity of the fluid, ϕ is the dissipation term and S_i is the energy source term.

The above mentioned equations describes the motion of a fluid in three dimensions. They contain a set of often unknown variables like temperature, density and pressure which needs to be considered. A way of linking the connection between the variables in compressible flows is by incorporating the equation of state. Equation 4 shows the standard form and equation 5 is a simplification and applicable for an ideal gas.

$$P = P(\rho, T) \quad \text{and} \quad i = i(\rho, T) \tag{4}$$

$$P = \rho RT \quad \text{and} \quad i = C_v T \tag{5}$$

P is the pressure, ρ is density, R is the universal gas constant.

The transport of species is solved for the mass fraction of all the species in the domain and is defined as

$$\Upsilon_m = \frac{M_m}{M_{tot}} = \frac{\rho_m}{\rho_{tot}}, \tag{6}$$

where M_m is the mass of species m in the cell, M_{tot} is the total mass in the cell, ρ_m is the density of species m, and ρ_{tot} is the density of the cell. This equation can be solved differently depending on the problem, either alone or together with any transport equation. Convection will not be considered in the species transport equation if momentum is not solved, and if so the species conservation equation will only contain diffusion terms. The compressible form of the the species conservation equation can be written as

$$\frac{\partial \rho_m}{\partial t} + \frac{\partial \rho_m u_j}{\partial X_j} = \frac{\partial}{\partial x_j}(\rho D_m \frac{\partial \Upsilon_m}{\partial X_j}) + S_m, \tag{7}$$

where

$$\rho_m = \Upsilon \rho \tag{8}$$

and u is velocity ρ_m is the species density, D_m is the molecular mass diffusion of species m and S_m is the source term which accounts for e.g evaporation and other submodels.

2.1.2   Reynolds-Average Navier-Stokes (RANS)

The Navier-Stokes equations (1,2,3) are solved in a time-averaged manner using this approach, which decomposes the instantaneous quantity into its time-averaged and fluctuating quantities. An idea first proposed by Osborne Reynolds [27]. The flow variables of the original Navier-Stokes equation are replaced by the following mean terms:

$$\mathbf{u} = \mathbf{U} + \mathbf{u'} \qquad p = P + p' \tag{9}$$

Where $\mathbf{u}$ includes the velocities u, v and w and p is the pressure.

The continuity, RANS equations and the scalar transport equation yield the turbulent flow equations for compressible flow, and is as follows:

Continuity:

$$\frac{\partial \bar{\rho}}{\partial t} + div(\bar{\rho}\tilde{U}) = 0 \tag{10}$$

RANS:

$$\frac{\partial \bar{\rho}\tilde{U}}{\partial t} + div(\bar{\rho}\tilde{U}\tilde{\mathbf{U}}) = -\frac{\partial \bar{P}}{\partial x} + div(\mu\nabla\tilde{U}) + [-\frac{\partial \left(\overline{\bar{\rho}u'^2}\right)}{\partial x} - \frac{\partial \left(\overline{\bar{\rho}u'v'}\right)}{\partial y} - \frac{\partial \left(\overline{\bar{\rho}u'w'}\right)}{\partial z} + S_{Mx} \tag{11}$$

$$\frac{\partial \bar{\rho}\tilde{V}}{\partial t} + div(\bar{\rho}\tilde{V}\tilde{\mathbf{U}}) = -\frac{\partial \bar{P}}{\partial y} + div(\mu\nabla\tilde{V}) + [-\frac{\partial \left(\overline{\bar{\rho}u'v'}\right)}{\partial x} - \frac{\partial \left(\overline{\bar{\rho}v'^2}\right)}{\partial y} - \frac{\partial \left(\overline{\bar{\rho}v'w'}\right)}{\partial z} + S_{My} \tag{12}$$

$$\frac{\partial \bar{\rho}\tilde{W}}{\partial t} + div(\bar{\rho}\tilde{W}\tilde{\mathbf{U}}) = -\frac{\partial \bar{P}}{\partial z} + div(\mu\nabla\tilde{W}) + [-\frac{\partial \left(\overline{\bar{\rho}u'w'}\right)}{\partial x} - \frac{\partial \left(\overline{\bar{\rho}v'w'}\right)}{\partial y} - \frac{\partial \{\left(\overline{\bar{\rho}w'^2}\right)}{\partial z} + S_{Mz} \tag{13}$$

Scalar transport:

$$\frac{(\partial \bar{\rho}\tilde{\phi})}{\partial t} + div(\bar{\rho}\tilde{\phi}\tilde{U}) = div(\Gamma_\phi\nabla\tilde{\phi}) + [-\frac{\partial \left(\overline{\bar{\rho}u'\phi'}\right)}{\partial x} - \frac{\partial \left(\overline{\bar{\rho}v'\phi'}\right)}{\partial y} - \frac{\partial \left(\overline{\bar{\rho}w'\phi'}\right)}{\partial z}] + S_\phi \tag{14}$$

For the above-mentioned equations, the overbar indicates a time-averaged variable and the tilde indicates a density-weighted variable. ϕ is the scalar.

2.1.3 Turbulence models

Turbulent flow can be characterized by its unstructured, chaotic flow field and is also differentiated from laminar flow by its large Reynolds number. The chaotic nature of turbulent flows has been an unresolved problem for a long time and it lacks physical clarifications, which is in contrast to laminar flow where physics are easier to comprehend. However, we do have turbulence models that can accurately characterize most flows. For the purpose of CFD analysis, it's crucial to pick the right model to describe the turbulence caused by a respiratory event like a cough, breath, or sneeze. The most used approach for this application is RANS and LES. Of these two RANS is the most popular due to it's relatively accurate results and at the same time low computational demand. The results from LES provides more accuracy, but are more costly in terms of computer power.

The RANS approach provides a variety of turbulence models that are categorised according to the amount of supplementary transport equations that must be solved along with the RANS equations, essencially, zero equations, one equation, two equations and seven equations. Among the most popular are k-ε and SST k-ω, where both use two additional equations to solve the kinetic energy (k) and the dissipation rate ε, and kinetic energy (k) and the specific dissipation rate (ω) respectively. The difference between these models lies in the near-wall performance, where k-ε is unsatisfactory for boundary layers with adverse pressure gradients. The k-ω model was suggested to resolve this issue by transforming the k-ε equation into k-ω equation in the near-wall region. This is done by transforming the ϵ equation into a ω equation by substituting $\varepsilon = $ kω. Both models has multiple submodels that can be used based on the problem, including standard k-ε, realizable k-ε, RNG k-ε, Wilcox k-ω and Menter SST k-ω among others. [28]

However, for multiphase flow problems the realizable k-ε is reliable and is the model used in the problem setup in this thesis. The realizable method differs from the standard method in two ways. Firstly, the turbulent viscosity is no longer a constant, but computed by a new eddy-viscosity equation. Secondly, the dissipation rate (ϵ) is derived from an exact equation for the transport of the mean-square vorticity fluctuation which results in a new transport equation for the dissipation rate. This provides improved performance in jets and mixing layers, separated flow and boundary layers compared to the standard method [29]. The transport equation for kinetic energy for standard k-ε and RNG k-ε is the same as for the realizable k-ε, shown in equation 15, but the turbulent viscosity is no longer constant, as mentioned. The viscosity expression itself is the same, but the model constant C_μ is different, see equation 16. Equation for turbulent dissipation is shown in equation 17 below [30].

$$\frac{\partial \rho k}{\partial t} + \frac{\partial \rho u_i k}{\partial x_i} = \tau_{ij} \frac{\partial u_i}{\partial x_j} + \frac{\partial}{\partial x_j} + \frac{\mu + \mu_t}{Pr_k} \frac{\partial k}{\partial x_j} - \rho \varepsilon + \frac{C_s}{1.5} S_s \tag{15}$$

S_s is the source term that represents the interaction with the discrete phase and Pr_k is the Prandtl number.

$$C_\mu = \frac{1}{A_0 + A_s \left(\frac{kU*'}{\varepsilon}\right)} \tag{16}$$

U* is the fiction velocity which is a function of strain rate and the rotation rate, A_0 and A_s are model

constants.

$$\frac{\partial \rho \varepsilon}{\partial t} + \frac{\partial (\rho \mu_i \varepsilon)}{\partial x_i} = \frac{\partial}{\partial x_j}\left[\left(\mu + \frac{\mu_t}{\sigma_\varepsilon}\right)\frac{\partial \epsilon}{\partial x_j}\right] + C_1 \rho \varepsilon S - C_2 \rho \frac{\varepsilon^2}{k + \sqrt{\nu \varepsilon}} + C_{\varepsilon 3} \rho \varepsilon \frac{\partial \mu_i}{\partial x_i} + S_\varepsilon \tag{17}$$

C_1, C_2 and $C_{\varepsilon 3}$ are model constants and S is the user-supplied source t

Near wall treatment

To ensure a stable solution of the computational domain it is crucial that the turbulent flow in the boundary layer is predicted accurately, essentially using a wall function. the structure of the boundary layer consists of a thin sub-layer, a buffer layer and the boundary layer, also known as the log-layer. Ideally, the first cell from the wall should lie within the viscous sub-layer, however for complex geometries and flow patterns this is challenging to do because it would require very fine mesh. The mentioned wall function enables us to use a larger mesh near the the wall [31]. The parameter y^+ is used to distinguish between the different layers, and describes the non-dimensional distance from the wall to the first node from the wall. For the log-layer this value should lie within the range of 30 to 300. A visual representation of the law of the wall is shown in figure 1.
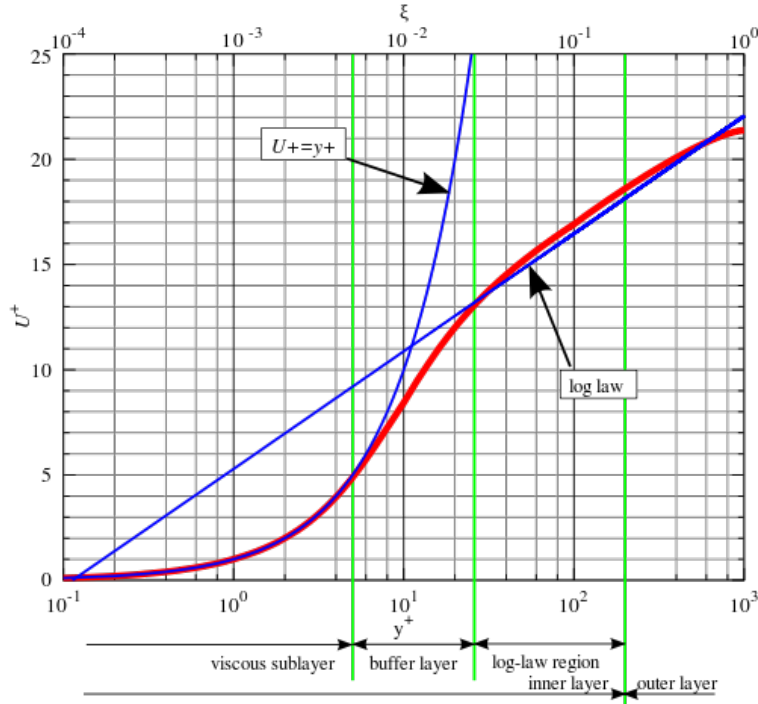

Figure 1: Average velocity distribution near a solid wall (law of the wall) [32]

The standard wall function is used in this thesis which applies the law of wall function. The law of wall function is based on u^+ and y^+ and the equations are shown in equation 19 and 20. Further, converge calculates the the shear velocity (u_T) as shown in equation 18 below:

$$u_\tau = \frac{|U_{i,tang}|}{\left(\frac{1}{\kappa}ln(E\frac{\rho u_\tau y}{\mu})\right)} \tag{18}$$

$$y^+ = y\frac{u_\tau}{\rho} \tag{19}$$

$$u^+ = \frac{u}{u_\tau} \tag{20}$$

Where $U_{i,tang}$ is the tangential velocity, κ is the von Karman constant, y is the distance to the solid contour and u is the velocity.

2.1.4 Eulerian-Lagrangian multiphase flow

A respiratory event such as breathing, coughing or sneezing is a flow pattern categorized as a multiphase flow. This is where the we have a combined flow that involves several phases, either gas liquid or solid. In the example of a cough, we have humid droplets intersecting the surrounding air, also referred to as a dispersed continuous phase interaction. A proper model is required to be able to adapt the characteristics of a respiratory event in to a model perspective. There are several models available for choice, and among the most popular mathematical approaches for this types of applications are the volume of fluid model (VOF), Eulerian-Eulerian model and Eulerian-Lagrangian model. The latter will be used in this thesis to describe the fluid motion of a respiratory event.

The Eulerian method of describing fluid motion is based on the consideration of a finite control volume in a defined domain, through which fluid particles flows in and out of. This is in contrast to the Lagrangian description of fluid motion, where we track the position and velocity of each fluid particle through space and time. The motion of a particle is obtained from its equation of motion shown in equation 21.

$$\rho_l V_d \frac{dv_i}{dt} = F_{d,i}, \tag{21}$$

where ρ_l is the liquid density, V_d is the drop volume and $F_{d,i}$ is the sum of the drag forces and the gravitational forces, which is described in equation 22 as

$$F_{d,i} = F_{drag,i} + F_{g,i} = C_D A_f \frac{\rho_g |U_i|}{2} U_i + \rho_l V_d g_i, \tag{22}$$

11

and

$$U_i = u_i + u'_i - v_i. \tag{23}$$

A_f is the drops frontal area, ρ_g is the density and U_i, u'_i and v_i is the local mean velocity and the turbulent fluctuating gas velocity, as seen in equation 23. The coupling between liquid and gas is important for an accurate spray modeling and therefore the drop drag is a crucial factor considered in the simulations, this accounts for the discrete liquid phase and the continuous gas phase and the interaction between the phases. Converge uses the nearest node approach to exchange of mass, momentum and energy of a Lagrangian particle with the Eulerian fluid phase values of the computational node that it is closest to [33].

Complex physical processes like droplet evaporation, droplet breakup and collisions needs considerations when analyzing spray behaviour in a multiphase flow setup. RH and temperature will affect the evaporation rate of the droplets, and have a significant effect on the droplet behaviour. Breakup is a phenomena of droplets occurring when the ambient forces (wind, drag etc.) are bigger than the surface of the droplet and "breaking" the droplet into smaller spherical volumes, essentially creating the spray phenomena as we know it. Due to the chaotic nature of sprays, also collision of droplets, describing the physical interactions and the shaping of droplets involving coalescence, stretching and bouncing, as well as wall interactions must be taken into account.

2.1.5 Computational fluid dynamics

CFD refers to a computer-based simulation of systems involving fluid flow, heat transport, and similar phenomena based on numerical analysis. This is a powerful tool for analyzing complex problems that would require big amounts of resources to accomplish for the same real-world experiment. However, CFD analysis cannot completely eliminate physical testing procedures because the need for verification of the analysis is necessary. There are various CFD softwares to chose from, each with their own set of strengths. They all have the same three main elements in common: 1) a pre-processor, 2) a solver and 3) a post-processor [34].

The pre-processor is responsible for defining the inputs for the current flow problem. Importing or generating an appropriate and operator-friendly geometry that the solver can handle is an important part of this process. Assumptions are made concerning the type of flow to be modelled, which includes defining fluid properties, selection of physical phenomena, boundary conditions and creating a suitable mesh for our domain. The mesh can be described as the control volume or cell where the properties of interest are solved, specifically at each node located in each cell. A large number of cells results in better accuracy but at the same time requires huge amount of computational resources, which is often a limiting factor. The meshing procedure in this thesis is built on the concept of adaptive mesh refinement, which will be discussed later [34].

The solver refers to the actual computation and how its done by the software. The numerical solution technique varies between softwares, with the finite volume method being the most popular. In general this involves integration of the governing equations of fluid flow in our domain, discretizing the integral equations into a set of algebraic equations and solving these by an iterative method [34]. In regards to this thesis, a high performance computer (HPC) is used to handle the computation of the problem setup allowing us to expand the complexity of the simulations for more accurate results.

The post-processing phase is where the results are visualized and analyzed. Through visual and/or graphical representation of the results we can verify and conclude. Most CFD softwares has built-in tools for this purpose including domain geometry and grid display, vector plots, contour plots etc. Converge also offers these tools, but with the use of HPC the attained output files are easier to post-process in Tecplot, which is used here. Tecplot specializes in visual data analysis tools that represents the experimental results in an efficient way [35].

2.1.6 Finite volume method

The basis of the numerical technique for the simulations is the finite volume method. This solves the properties at the center of each cell according to the summed fluxes through the cell faces and an internal source term. The governing equations is solved iteratively using a set of nonlinear coupled second-order partial differential equations. FVM offers advantages over other techniques mainly by how the integration of the control volume is achieved. The resulting statements express the conservation of relevant properties for each finite size cell leading to a clear relationship between the numerical algorithm and the underlying physical conservation principle. This makes the concept simpler to understand. The conservation of general flow in and out of a control volume can be described with the following balance:

$$\frac{\partial \phi}{\partial t} = \phi_{convection} + \phi_{diffusion} + \phi_{source} \tag{24}$$

where ϕ is a general flow variable [34].

The process of solving governing equations incorporates an iterative algorithm, as mentioned. For most flows, the scalar variables due to convection are unknown. The scalar dependencies on the magnitude and the direction of the local velocity field creates the need for a strategy to solve the flow variables [36]. This thesis employs Pressure Implicit with Splitting of Operator method (PISO) for the coupling of pressure and velocity. This method employs one predictor step and two corrector steps, enhancing the SIMPLE algorithm with one additional corrector step. Here, a guessed value of the pressure (p*) are used to give the velocity components (u*, v*) to solve the discretized momentum equations. Through multiple correction steps we get twice-corrected pressure field as shown in equation 25.

$$p^{***} = p^{**} + p'' = p* + p' + p'' \tag{25}$$

Where p** is the correct pressure for the first corrector step, p" is the pressure correction for the second corrector step, p* and p' is the initial guess of the pressure and the correction for the first correction step, respectively.

2.1.7 Ventilation strategies

MV and DV are two common mechanical ventilation strategies used to bring fresh air into buildings to ensure a good indoor environment, each with its own set of benefits and drawbacks. MV is a conventional air distribution method for regulating the indoor environment, in which fresh air is supplied at a high velocity from the ceiling level to achieve a complete mixed environment and an even temperature throughout the room. It is supplied outside of the residence zone to avoid draft.

With DV, the air is fed with a low velocity directly into the residence zone and the cold supply air is distributed evenly across the entire floor. The principle is based on the buoyancy effect, which causes the cold supplied air to rise near heat sources in the room (humans, technical equipment, etc.). The heat from the heat sources will lift the fresh air upwards, removing many of the pollutants and distributing it evenly throughout the space. This strategy works well in bigger areas like libraries, cinemas, conference halls etc. The suppliers are usually places near floor level. Figure 2 illustrates both MV and DV scenarios.
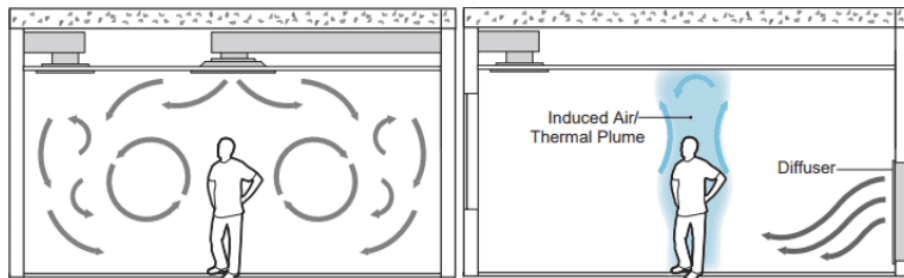

Figure 2: Mixing vs displacement ventilation taken from [37]

2.2 Model description and problem setup

This section will describe the background of the CFD simulations. The key area of investigation is how the ejected respiratory droplets from various respiratory events (cough, speech and breathing) are affected by the surrounding airflow, essentially from mixing ventilation and displacement ventilation, as well as different ACH. The potential for airborne transmission of virus-carrying droplet nuclei as a result of evaporation is of particular interest. This is implemented through a user-defined function (UDF) which ceases evaporation of droplets smaller than a radius of 2.5 μm.

Scenarios involving breathing, coughing and speaking are studied across two models with different air flow patterns and air flow rates i.e., MV with low and high ACH, and DV with low and high ACH. A total of 5 cases are studied where cases 1-4 are simulated for 120 s and case 5 is simulated for 30 s involving human motion. A sequence of respiratory events are conducted between the persons resembling a realistic scenario of coughing, breathing and speaking in an office. In terms of the respiratory sequence, two different sequences are applied to the persons depending on the case. Both sequences of breathing, speaking, and coughing lasts for a total of 30 s to analyse the dynamics of each respiratory events. For cases 1-4, the simulation continues from 30 s to 120 s without any further injected particles, to analyze the evolution of the particles in the indoor space. Sequence 1 applies to cases 1 through 4 and sequence 2 applies to case 5. The sequences are described below. The persons are labelled as shown in figure 4 and figure 5.

Sequence 1 starts with two breath cycles (exhale - inhale) for both person one and two. At 10 s, person one starts speaking from 10 s to 20 s, then breathes continuously until 30 s. Person two initiates a cough at 10 s, followed by continuous breathing until 30 s is reached. For sequence 2, an additional person is added to the model (person three), with the purpose of walking in a straight line from the chair at person one's desk towards the opposite wall while speaking and breathing. Sequence 2 is as follows. Person one starts breathing two cycles until 10 s, then starts speaking from 10 - 20 s followed by continuous breathing until 30 s. Person two breathes similar to person one for 10 s, then coughs once at 10 s, followed by continuous breathing until 30 s. Person three starts with breathing until 20 s, followed by speaking from 20 - 30 s in combination with walking at a velocity of 0.5 m/s. The respiratory sequences are shown in figure 3.

All the cases are completed with a relative humidity of 50 %. The supply air flow rate is determined using the Norwegian regulations for office buildings [38], assuming the room is designed for two persons with low activity and low material emissions, resulting in a total air flow at 107 m^3/h, corresponding to an ACH of 1.62. For the cases with higher ACH the air flow is simply doubled, resulting in 214 m^3/h or ACH of 3.2. See appendix J. The supply air temperature is set to 20 °C. Cases are summarized in table 1.

Table 1: General overview of the cases

Case no.	Sequence	Ventilation strategy	ACH	Sim. time [s]
1	1	MV	1.6	120
2	1	DV	1.6	120
3	1	MV	3.2	120
4	1	DV	3.2	120
5	2, with human motion	MV	1.6	30
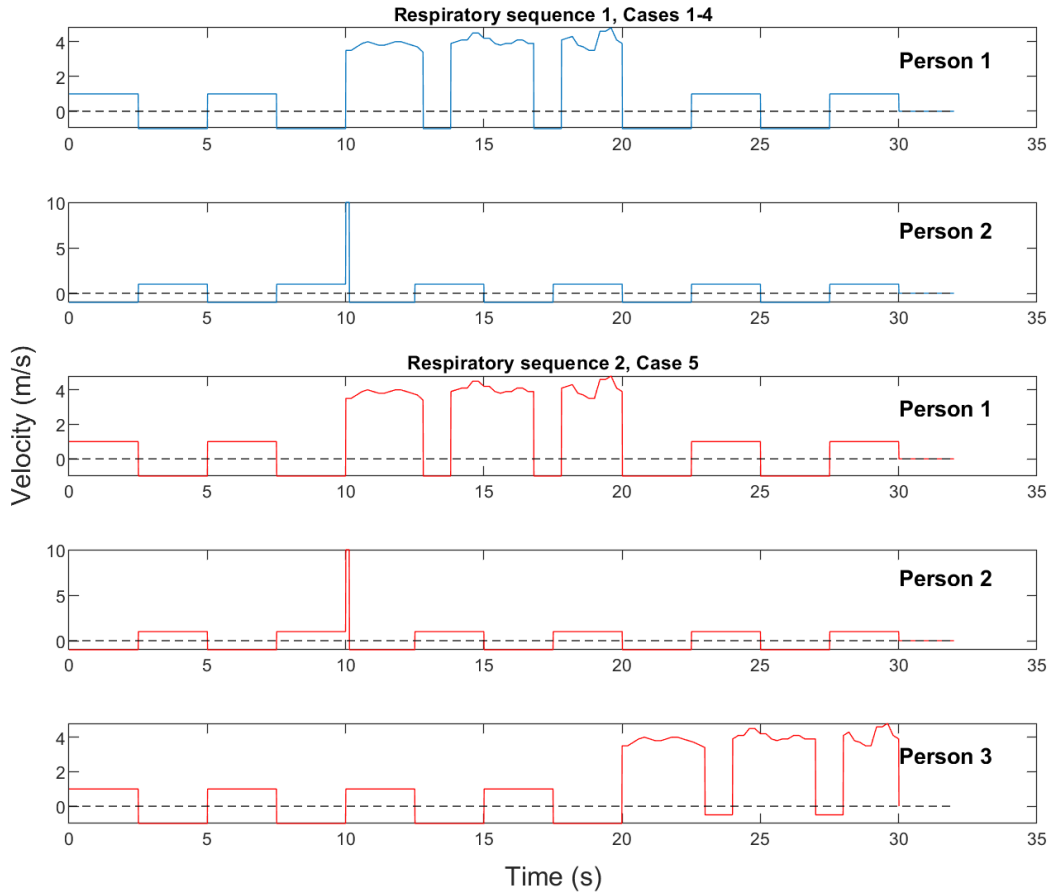
Figure 3: Respiratory cycles for scenario one and two

We consider a small double-office shaped as a rectangular box. The dimensions of the model is 5.5 m x 4 m x 3 m (L x W x H). For the displacement ventilation, there are two identical inlets located near the floor at the east wall, each with an area of $0.42\ m^2$. The model with mixing ventilation has the inlet located in the ceiling with an area of $0.4\ m^2$. The outlet is identical for both cases, located above the door with an area of $0.4\ m^2$. To handle undesirable backflow, the outlets are modelled as 1 m long ducts. Figure 4 and 5 shows a visual representation of each room.

Figure 4: Model setup, mixing

Figure 5: Model setup, displacement

There are two box-shaped persons sitting on their own desk having a total surface body area of 1.90 m^2 as well as a standing person with an area of 1.84 m^2 [39]. Person one is rotated 90° facing person two. Table 2 summarizes the geometries of the persons, and visuali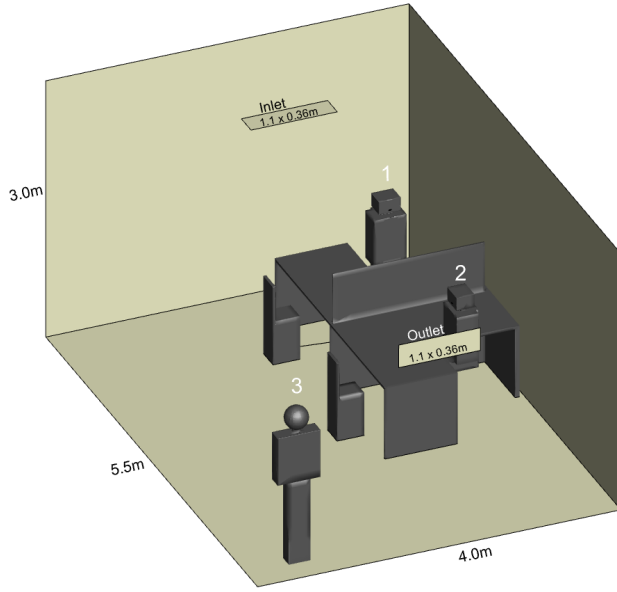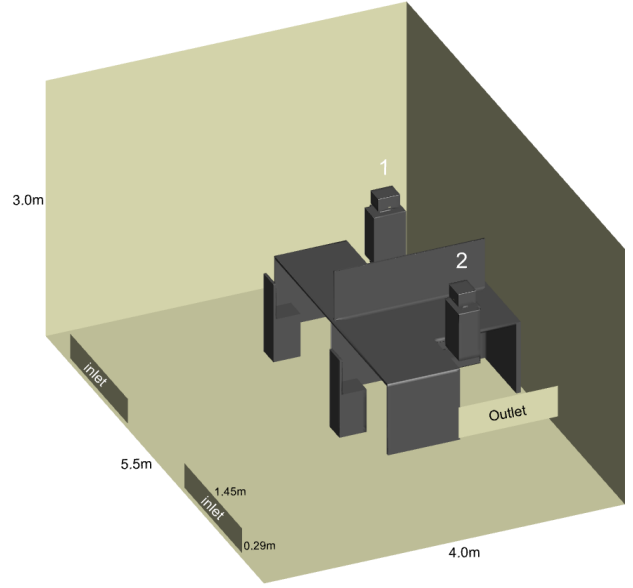zation is shown in figure 6. The area of the mouth differs depending on the type of respiratory event. For breathing instances an area of 1-1.2 cm^2 and for coughing instances an area of 3-4 cm^2 is regularly used by existing studies [40], [41]. Based on this, a mean area of 2.4 cm^2 is used in this model with a rectangular shape. The geometries were created using Sketchup 2022, and imported as .STL files into Converge Studio. The Sketchup models are attached in appendix C.

Table 2: Geometry of the modeled persons

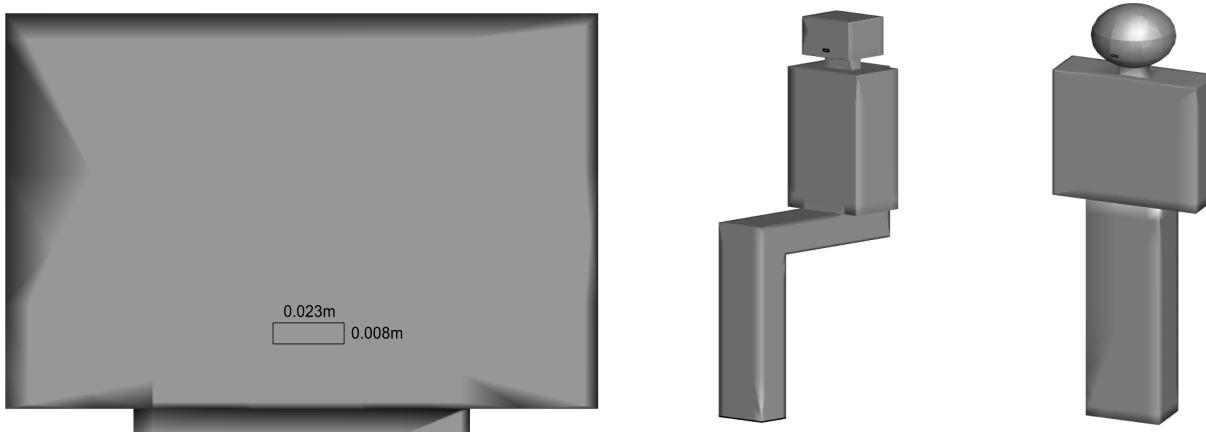| Sitting person	Dimensions [L × W × H]	Unit
Mouth	0.028 x 0.08	m
Neck	0.05 x 0.14 x 0.05	m
Body	0.24 x 0.36 x 0.55	m
Legs	0.22 x 0.14 x 1.24	m
Chair (back)	0.03 x 0.22 x 0.55	m
Head	0.2 x 0.24 x 0.15	m
Standing person	Dimensions [L × W × H]	Unit
Mouth	0.028 x 0.08	m
Neck	0.07 x 0.07 x 0.05	m
Body	0.15 x 0.47 x 0.55	m
Legs	0.15 x 0.24 x 0.95	m
Head	0.25 (diameter)	m

Figure 6: Geometry of the head, sitting and standing person

2.2.1 Steady state modeling

To be able to capture the transient behaviour of the emitted droplets from a respiratory event, a steady state solution of the setup was established as a first step. Because a respiratory event lasts for only a short duration, a steady state model must be achieved in advance to establish the desired flow fields and relative humidity in the room. This allows for a more efficient investigation of the emitted droplet's behavior, as well as how they are affected by the surroundings. The solution of the steady state simulation is utilized as the initial state for the transient simulations with respiratory events

Grid control

Creating a mesh means that the defined computational domain within the simulation is divided into smaller control volumes, also referred to as creating a grid. To be able to compute desired flow field it is evident that the mesh is fine enough to capture the location in our geometry expected to have the greatest change of variable. As mentioned in section 2.1.5 the amount of mesh in our domain determines the accuracy and the computational costs of our simulation, meaning we have to adjust the mesh accordingly to achieve both high accuracy in the location of interest and at the same time low computational cost. The mesh in the steady state simulation is fixed, in oppose to the transient spray simulation where AMR is utilized. This will be explained further in section 2.2.2.

The mesh of the geometry is set up by choosing a base grid that fits the geometry. This is set to 0.1, resulting in a total cell count of 65820 without embedding or AMR. The embedding is specified separately for each boundary depending on the wanted resolution. Number of embed layers is set to 1 and scale is set to 1. More embedding results in lower y^+ due to higher grid resolution near the wall. Figure 7 shows the embedding, which is similar in each model.
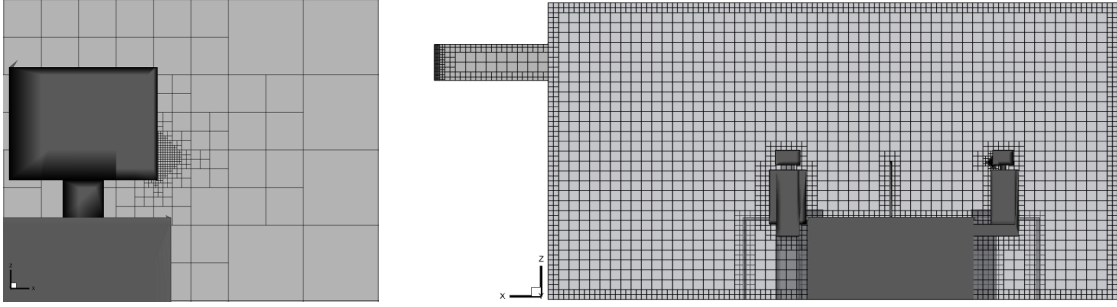
Figure 7: Embedding of the mouth and the room

Boundary conditions

Establishing proper boundary conditions is a critical step of setting up the model. The boundary conditions used for the steady state simulation are summed up below:

The DV model has two inlets on the lower part of the same wall with identical geometry and boundary conditions. They are modelled as Dirichlet inflows with velocity boundary conditions specified to 0.0354 m/s and 0.0708 m/s, depending on the case, in their respective direction, y, and the temperature is set to 22 °C. The MV model has the inlet located in the roof, with the exact same boundary conditions except for an inflow velocity of 0.0743 m/s or 0.148 m/s. Species at the boundaries are set to N_2, O_2 and H_2O with fractions corresponding to a relative humidity of 50 %, 0.760775, 0.231109, and 0.008116 respectively. Turbulent kinetic energy (κ) is specified in terms of turbulent intensity and set to a fraction of 0.066 for DV and 0.058 for MV. Turbulent dissipation (ϵ) is specified in terms of length scale and set to 0.033m for DV and 0.038m for MV. Calculations are shown in appendix F.

The exhaust is set to a Dirichlet outlet with atmospheric pressure, 101325 pa and zero normal gradient. Velocity boundary condition is stationary with the law of wall incorporated for the walls, roof and floor. The temperature condition is heat flux specified at 0 W/m^2. Zero normal gradient is chosen for the (κ) and global near wall treatment for the (ϵ). The wall functions of turbulence models acts desirably with this setting. The persons are modelled as stationary wall boundaries, with specified temperature boundary at 32 °C [42] .

Relative humidity

The relative humidity (RH) for the room is not possible to specify directly and has to be specified in terms of mass fractions of air, N_2, O_2 and H_2O. Higher fraction of H_2O will result in a higher relative humidity. The calculations reflects a RH of 50 % with the input values shown in table 3 below. Complete calculations are shown in appendix E.

2.2.2 Spray modeling

As mentioned in the previous section, the gas and discrete phase of the spray event was modeled with an already established steady flow field in the room. The respiratory events consisting of coughing and

19

Table 3: Overview of relative humidity input values

Relative humidity		
Room temperature	T_room [°C]	22
Relative humidity room	RH_room [%]	50.0
Molar mass H_2O	Mm_H_2O [g/mol]	18.01528
Molar mass air	Mm_air [g/mol]	28.96470
Saturated vapor pressure	P_sat [kPa]	2.644203
Vapor pressure	P_H_2O [kPa]	1.322102
Mole fraction vapor	γ _H_2O	0.013048
Mole fraction air	γ _air	0.986952
Mass fraction H_2O	ω _H_2O	0.008116
Mass fraction O_2	ω _O_2	0.231109
Mass fraction N_2	ω _N_2	0.760775
SUM MASS FRACTIONS		1.0

speaking are modeled with breathing instances for a more realistic approach. The particles are tracked using the Lagrangian method.

Boundary conditions of the mouth
In the steady state simulations, the mouths were modeled similarly to the walls. Additional boundaries for each persons mouths are added to create the continuous gas phase from the mouth. They are modeled as inflows with velocity boundary conditions specified as a profile configuration consisting of air, that is N_2 and O_2. The velocity configuration varies depending on each person's chosen respiratory sequence, as described in section 2.2. Based on existing studies on coughing the velocity is set to 10 m/s [43, 44, 45], for breathing it is set to 1 m/s [46] and for speaking it is set to a mean of 4 m/s [44]. To account for the velocity of the walking person, the velocity for the mouth boundary while walking is increased 0.5 m/s to ensure that the relative velocity is similar. The nature of a speech is fluctuating between different velocities, and therefore the velocity is set accordingly. Complete velocity profile configurations for both sequences per person are shown in appendix G.

Ejection time for the cough is 0.12 s [7], breathing is 5 s in total with 2.5 s of inhale and 2.5 s of exhale [47] and the speech represents a person speaking for 10 s with two inhales of 0.8 s within the time-span. Each persons respiratory cycle is shown in figure 3.

Injectors and nozzles
To be able to combine two respiratory events, each person is modelled with two injectors representing either cough, breathe or speech. The injectors are positioned at the mouth area each consisting of one nozzle. To determine the nozzle diameter the following equation is used, depending on velocity and density of the injected particles and mass and time of the injection:

$$D = \sqrt{\frac{4 \, m}{\rho \, v \, dt_{inj} \, \pi}} \tag{26}$$

To combine coughing and speaking with a breathing sequence at the same boundary (mouth), person one and

20

two is modelled with two injectors representing either cough, breathe or speech. Person one and three has one injector with the rate shape corresponding to the speech and one injector with rate shape corresponding to the breathing sequence, determined by the velocity boundary profile, mass and nozzle diameter for each respiratory instance. Person two follows the identical procedure, with one injector for cough and one for breathing. The rate shape is set to achieve an even distribution of mass of the exhaled droplets at the correct time steps for the different instances. Figure 8 shows the placement of the nozzles.
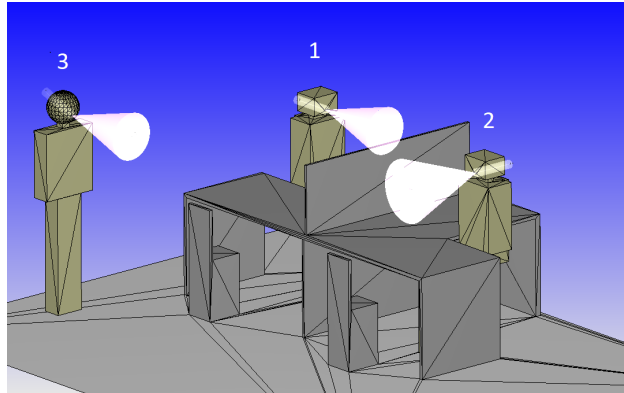

Figure 8: Placement of the nozzles

For breathing (one exhale), one cough and speech, the nozzle diameters are 0.00406 mm, 0.08955 mm and 0.007642 mm, respectively. Calculations are shown in appendix A. in addition, the nozzle has a spray cone angle of 40° for cough and 30° for breathing [47]. A speech varies in intensity over time depending on the magnitude of the sentence, as well as pronunciation, therefore the cone angle is set to a user-defined configuration where the angle varies over time. The angles are set to random numbers at different time steps between 30-45°. This is based on reasonable assumptions, as there are no earlier studies reporting on this topic. The speaking persons are simulated with the same configuration, as shown in figure 9 below. The temperature of the injections are 34°C, additional inputs for each respiratory sequence is shown in appendix B.
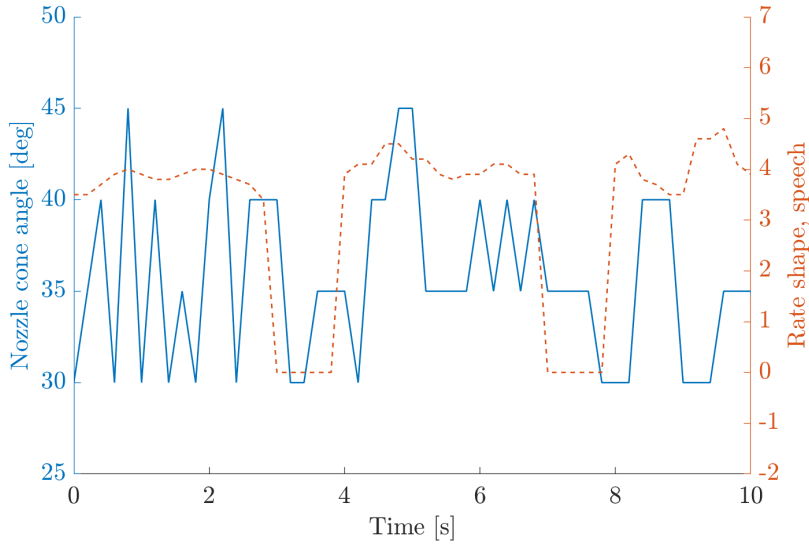
Figure 9: Profile configuration of the nozzles for speaking

Particle distribution

The spray particle distribution is introduced into the domain using parcels, which is a collection of identical drops with the same radius, velocity, temperature, and so on. The parcels represent the full spray field, resulting in a greatly reduced simulation computation time [48]. The number of injected parcels for one cough, one exhale and a 10 s speech is 3500, 1600 and 3000, respectively, with mass of each injection equal to 7.7 mg [9], 0.033mg [49] and 1.57mg [49]. Disagreement exists on the amount droplets and mass ejected from a cough, speech and breathing in the literature between different studies, the values are therefore chosen based on reasonable assumptions from the mentioned studies, as well as [50] and [51].

Injection size distribution for coughing is determined by the cumulative probability distribution by Rosin-Rammler which is based on the sauter mean diameter (SMD) for each respiratory sequence. SMD is a commonly used term in fluid dynamics, especially for sprays where the drops consists of different sized particles. Measurements of ejected particles will provide information on the fractions of different-sized drops which can be presented in terms of volume [52]. Dbouk and Drikakis found that the initial diameters of coughed droplets are between 30-90 μm [10], also Xie et al found that on average 40 % of the droplets were smaller than 75 μm from 20 coughs [49]. Based on these findings a SMD of 73 μm is used for cough.

Experiments on the distribution of droplets from breathing show small diameters, ranging from 0.1 - 5 μm [19]. A log-normal function with a mean diameter of 5 μm and a standard deviation of 0.5 is used to fit the distribution with the droplet sizes ranging from 0.3 - 15 μm.

For the speaking, potentially more droplets will be emitted as a result of the vocal folds vibrating. The number of droplets produced is determined by the intensity of the speech and the words pronounced, but will vary substantially from person to person due to different pronunciations. Regular speech is considered in

22

this thesis and the distribution is also fitted to the same log-normal function as with breathing. The droplet size is also an area of disagreement. Morawska et al found a mean diameter of 5 μm from speaking [53]. Another study by Duguid found initial sizes between 12-21 μm prior to dehydration [54]. The probability density function (PDF) and cumulative density function (CDF) for the distributions are shown in figure 10 and 11.
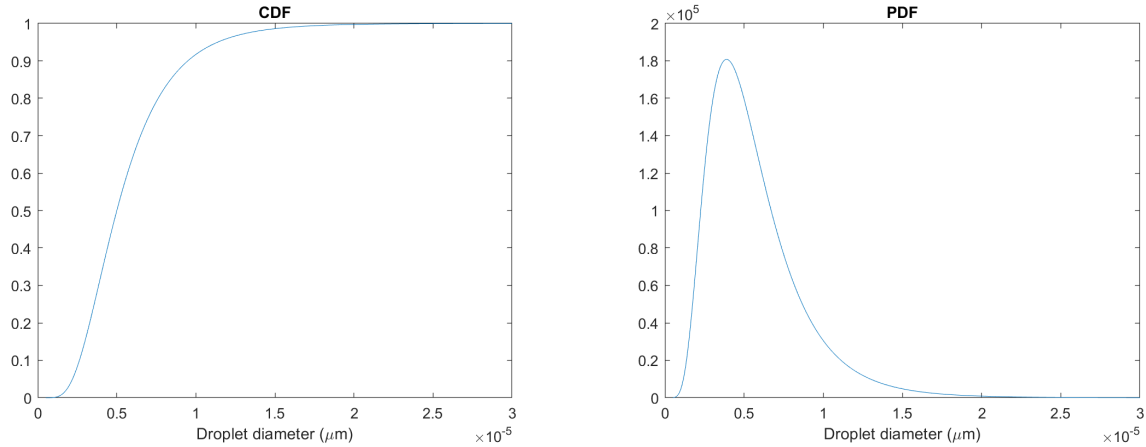

Figure 10: CDF for speech and breathing distribution   Figure 11: PDF for speech and breathing distribution

Droplet evaporation

The injected droplets are considered homogeneous droplets consisting of water. Once the liquid spray is injected into the domain, the droplets will evaporate. The Frossling model is utilized to account for this, essentially describing how the droplets radius changes over time. Because the rate of evaporation is affected by the room's temperature, relative humidity, and air movement, the evaporation model must also be used in conjunction with a temperature model that takes these factors into account - uniform temperature model.

The droplets will gradually evaporate into small droplet nuclei after some time, and due to their low mass they will follow a trajectory similar to the local air flow. A UDF has been integrated into the simulation making it possible to track the movement of the smallest droplets over time. The UDF code specifies that droplets smaller than or equal to a radius of 2.5 μm will cease to evaporate, as is it shown in various reports that droplets smaller than approximately 5 μm in diameter can remain airborne for a long time, potentially carrying infectious viruses [55, 56].

Droplet breakup

The drop breakup model used for the simulations is the combination of Kelvin-Helmholz and Rayleigh-Taylor instability (KH-RT). Here, a breakup length is specified where only KH instabilities are responsible for the breakup. When the particles have travelled beyond the specified breakup length either KH and RT are activated and responsible for the breakup, depending on which one are more suitable. For droplet collisions and coalescence the O'Rourke models is utilized.

Adaptive mesh refinement

Adaptive mesh refinement (AMR) is incorporated in the spray phase of the simulation to automatically adapt the accuracy of the solution in regions of interest. In the steady state simulation the calculations are limited to the pre-defined grids constituting the domain (specified in section 2.2.1), but with AMR we are able to acquire more accurate solutions in the region of interest without being limited to refining the grids in the entire domain. This method saves tremendous amount of simulation time and computational power. The AMR embedding is set to 3 and the mesh around the mouth area is also refined to a scale of 5 with an embedding of 10. Higher embedding gives better resolution, but it comes at a higher cost in terms of computing.

2.3   Submitting jobs to HPC

Numerical CFD simulations entail solving numerous equations for each cell in the domain, which necessitates a significant amount of computer processing power. The ability to process simulations on a high-performance computer allows for more thorough simulations and analysis. The process of submitting a job is handled through SSH secure shell client. This is a network protocol that ensures a secure way to access and share files related to the simulation.

To run a simulation, we first need to include the input files (.in) to the same folder. The .in-files includes boundary.in, spray.in, inputs.it among others, depending on the case setup and are exported from Converge Studio. They are created on notepad, making it convenient to change inputs after they are exported. The folder with .in-files is then copied to the respective "home" folder in the HPC folder-structures in the Linux terminal (SSH secure shell). In addition, a job submission file (sbatch) that consists of processing tasks must be created and submitted into the "home" folder. Here, we specify commands, resources (CPU), runtime and input and/or output files for the task to be carried out. An example of this file is shown in appendix I. The supercomputing facilities of Fram computer cluster (UiT Arctic University of Norway) under the project NN8005K at Notur, UNINETT Sigma2 AS (National infrastructure for scientific computational science in Norway) was utilized to run the simulations [57].

2.4   Creating the UDF

To run a simulation with user defined function, additional steps are required. We need a configuration tool (cmake), a build tool (make) and a system C compiler to create the UDF library. Header files and source files must be created according to the chosen UDF setup and can either be chosen from existing example files or user defined files can be created. Further, the source files must be compiled in the Linux terminal to generate CMakeLists.txt and "examples", "src", "include" and "build" directories. The UDF source files and header files must then be copied to the appropriate "src" or "include" folder. The next step is to generate the files we need to build the UDF library, this creates the libconverge_udf.so library [58]. The UDF for evaporation and motion requires the following files: load_lag_env.c, species_table_functions.c, spray_evap.c, spray_inject_custom.c, user_header.h and env.h. To be able to run the simulation with UDF, inputs.in and udf.in from the input files must be modified in accordance with the UDF setup we have. In inputs.in "udf_flag" must be set to 1, and in udf.in "user_evap_flag", "user_parcel_flag" and "user_spray_inject_custom_flag" must be set to 1. The simulation can then be executed using an appropriate sbatch file, which has to be modified to run with the UDF.

To build the UDF library on windows we need to use Microsoft Visual studio to compile the files. First, a working directory must be created including three subdirectories "src", "include" and "zx" (the latter folder can be named as you wish). "zx" includes "include", "lib" and "share" folders. CMakeLists.txt is then copied from the program files on the computer into the working directory. The header and source files are then copied into appropriate folders. Before using the build tool (CMake) to generate the build directory, it is important to modify the path within the .txt file to make sure it corresponds to the directory "zx". When the build folder is generated it must be compiled in Visual Studio to create "converge_udf.dll, which must be copied into the directory where the simulation is run. Similar to Linux, inputs.in and udf.in must be modified as well.

2.5 Verification of the model

The present work is a natural extension of the master's thesis from 2021 by Patrick Paulsen [11]. The implementation and verification of the UDF is first performed with an elevator setup similar to that investigated in [11]. The results are compiled and communicated as a conference article for SIMS 2022.

We incorporated breathing and coughing with UDF to cease evaporation at a radius of 2.5 μm, but kept the same model setup. This paper has been written in co-operation with Oda Martine Sundsdal. Preliminary results are shown in figure 12 below.

The results show the dispersion of the exhaled droplets in an elevator setup. The convection from the person is not considered in this setup, meaning only buoyancy and local air flow will affect the smaller particles trajectories (figure 12(a) and 12(b)). The coughed droplets are bigger and follows a ballistic trajectory depositing to the ground within a short time-span (figure 12(c)), whereas figure 12(d) shows the evolution of droplets at 19.5s after evaporation.
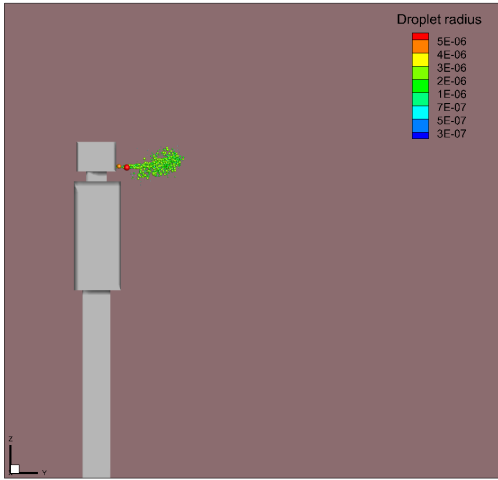
(a) Breathe at 1.7s
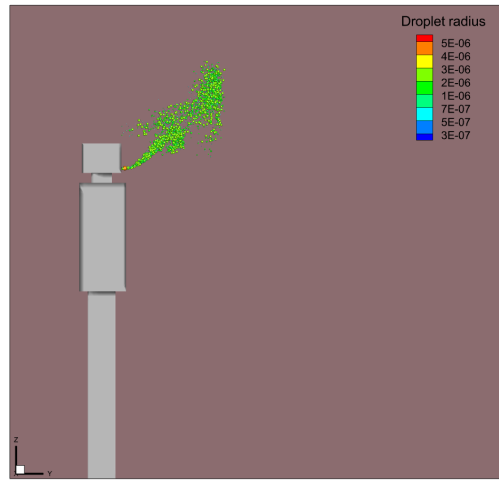
(b) Two breaths at 7.1s
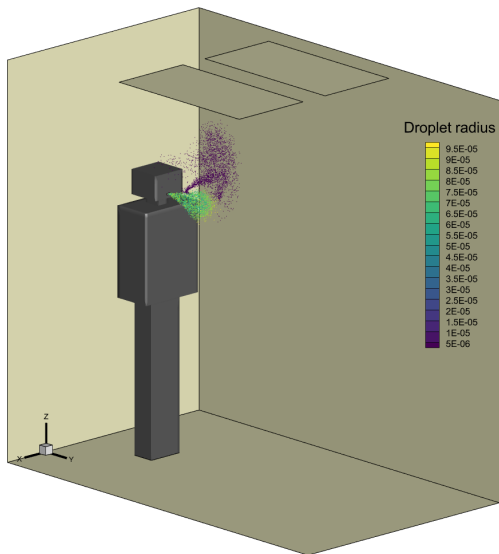
(c) Breathe and cough at 7.6s

(d) Breathe and cough at 19.5s

Figure 12: Evolution of droplets from cough and breathe with UDF as presented in the results for SIMS2022 conference

3   Results and discussion

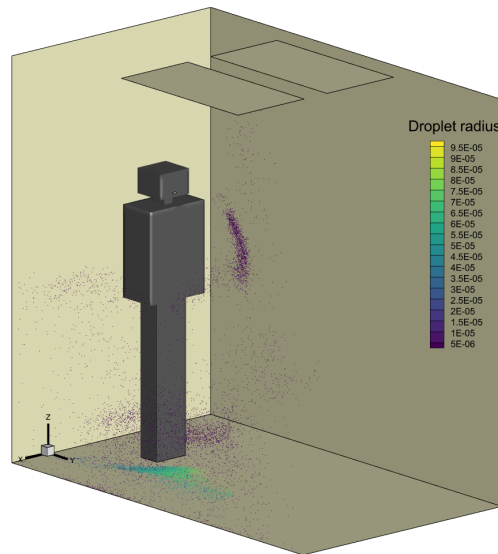This section will present the results from the numerical simulations. The study is conducted with the main purpose of investigating the different ventilation strategies and how the respiratory droplets behave within a confined space. Five cases are investigated as described in table 1 of section 2.2.

3.1   Steady state simulation

The steady state simulations are performed to establish the desired variables that influence the modeling of respiratory instances in the domain, such as flow fields, relative humidity, temperatures, and so on. For both the investigated domains, mixing ventilation and displacement ventilation, one steady state model has been developed with low flow rate (107 m^3/h or 1.6 ACH) and one with high flow rate (214 m^3/h or 3.2 ACH), 4 in total.

Figure 13 and 14 indicates that mass flow rate convergence is achieved within 8000 to 10000 cycles for MV and 4000 and 10000 for DV. The inlet mass flow rate for the MV case with ACH 1.6 reaches steady state at -0.03558 kg/s, with the outlet stabilizing at 0.0361 kg/s. For ACH 3.2 the inlet and outlet stabilizes at -0.07087. DV reaches steady state at -0.0353 kg/s for the inlet and 0.0360 kg/s at the outlet and for ACH 3.2 the inlet stabilizes at -0.0672 kg/s while the outlet stabilizes at -0.0675 kg/s. This corresponds to the inlet boundary conditions set in the models.

The minor difference in mass flow rate for the inlets and outlets is due a backflow at the outlet which only affects the flow within the duct, and not the domain of interest. The difference in mass flow for MV and DV is within 0.0007 at maximum and assumed negligible. See appendix D.
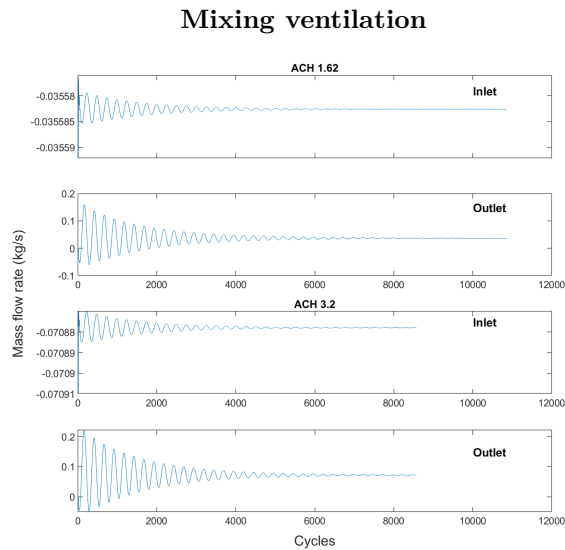
Figure 13: Mass flow rates, MV
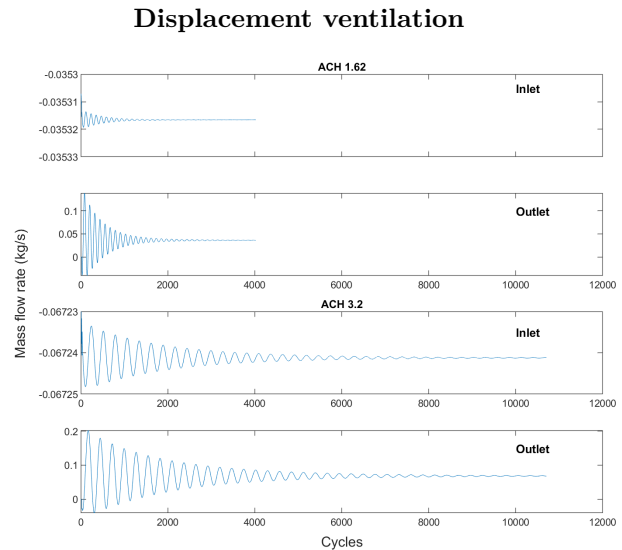
Figure 14: Mass flow rates, DV

Continuing with the flow field for MV and DV, which is represented by streamlines showing the velocity, as seen in figures 15, 16, 17, and 18 respectively. The models' flow fields show comparable behaviour clearly influenced by the heat convection plumes from the people in the room, creating an upwards flow around the persons towards the ceiling. The flow from DV shows the desired characteristics of such ventilation strategy. The cold supplied air is heated up in contact with internal loads (persons, technical equipment, lightning etc.), transporting pollutants/particles towards the ceiling where it is extracted. MV also shows a well mixed space, as desired. The difference in air velocity in figure 15 with 1.6 ACH and figure 16 with 3.2 ACH is showing clearly.

Figure 15: Steady state flow field for MV with ACH 1.6

Figure 16: Steady state flow field for MV with ACH 3.2
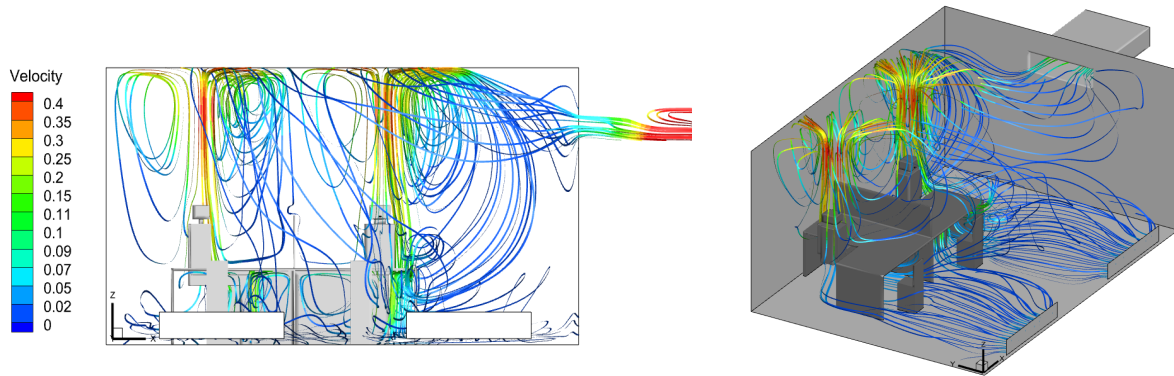
Figure 17: Steady state flow field for DV with ACH 1.6
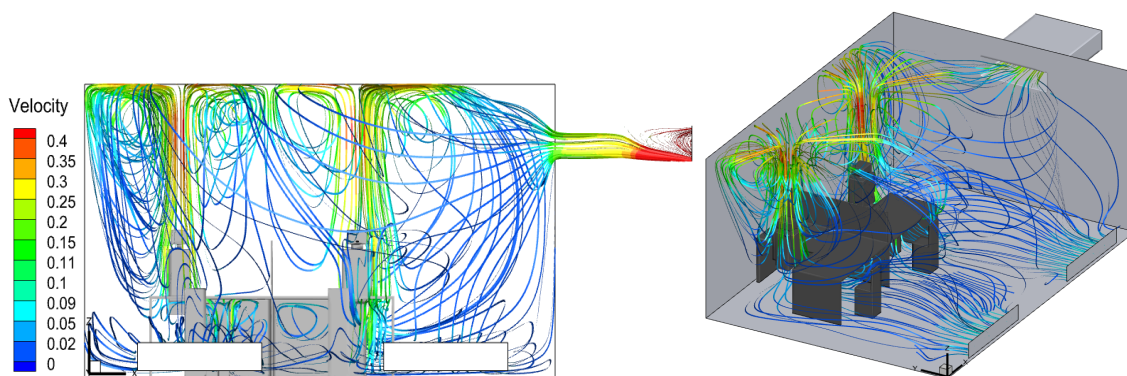
Figure 18: Steady state flow field for DV with ACH 3.2

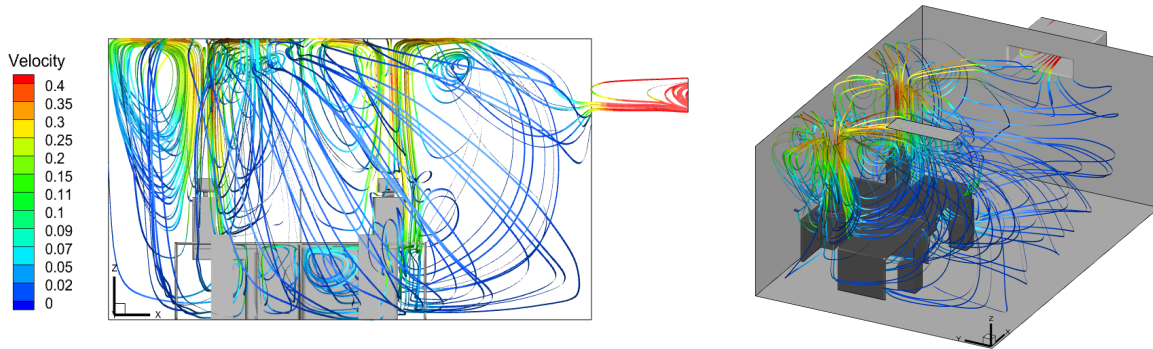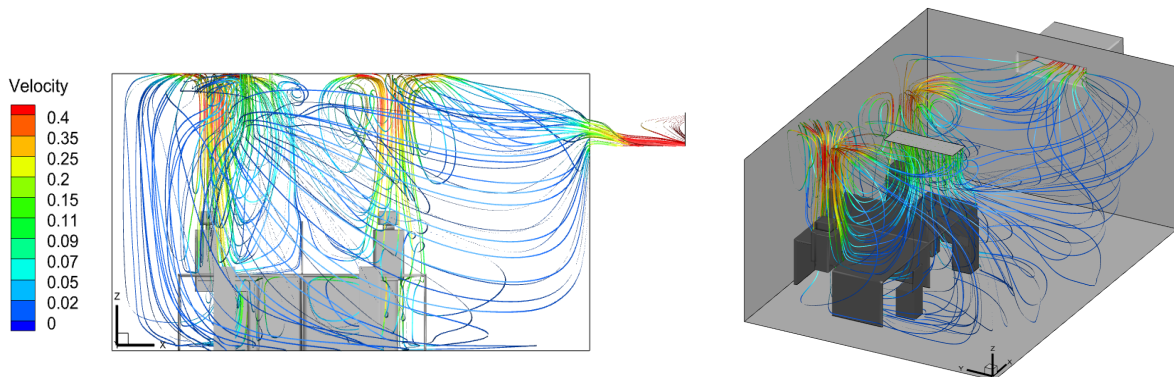Figure 19 shows the RH and y^+ for both models. The values are the same for MV and DV, therefore only the MV case is visualized. y^+ for both models is 20 - 30 and falls near the desired log-layer region of the turbulent boundary profile shown in figure 1. On a colour-coded scale, the resulting RH is also visualized, here at an RH in the mid 50's. The calculations and incorporation of RH is explained in section 2.2.1. The equations used in Tecplot to visualize the relative humidity is shown in appendix E.

(a) Y^+ for MV and DV

(b) Relative humidity for MV and DV
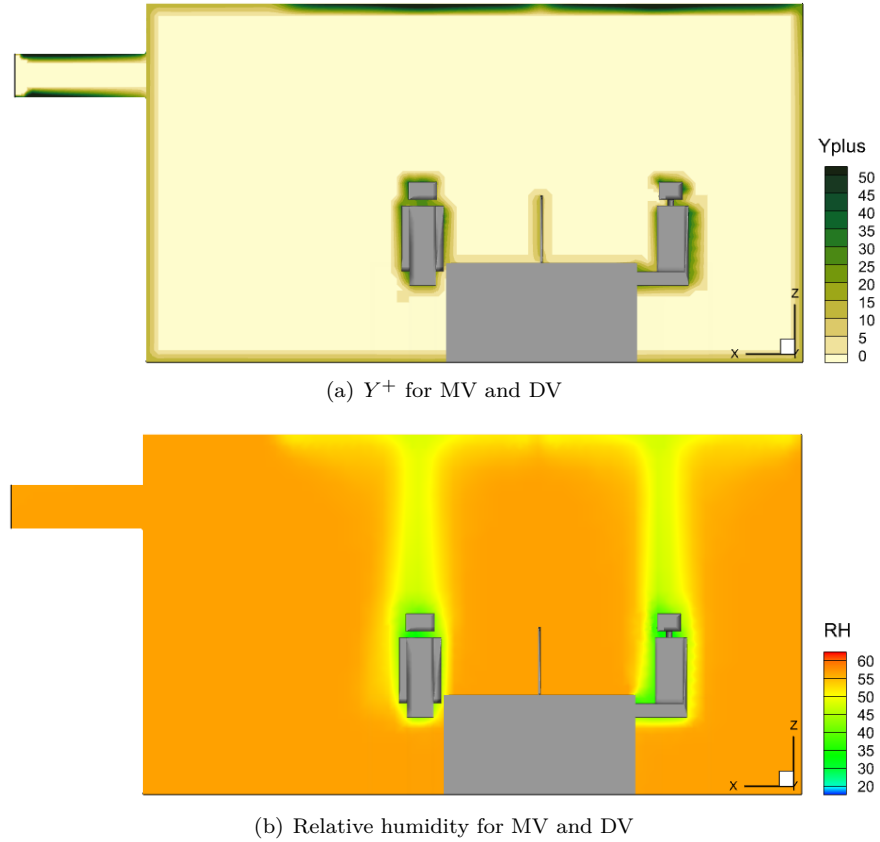
Figure 19: Illustration of Y^+ and relative humidity for MV and DV

Figure 20 shows a uniform temperature distribution throughout the room. The only source of heat in the room is the humans, who create a heated plume that extends around and above towards the ceiling. They are specified at 32 °C as this enables a more substantial visualization of the heat emitted from a person, in accordance with existing literature mentioned under the boundary conditions in section 2.2.1. The stratification of temperature is an important factor especially for displacement ventilation and is not accounted for in this thesis. The particles will be affected only by gravity, the thermal plume of the persons and the local air flow.
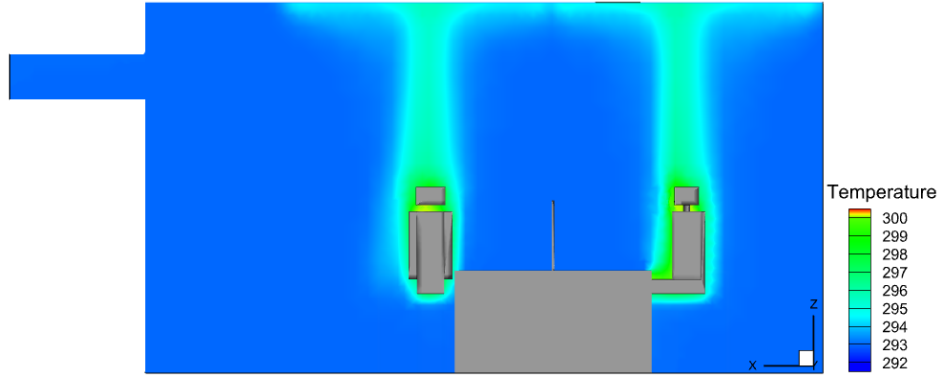
Figure 20: Temperature distribution, mixing and displacement

3.2 AMR

Figure 21 below shows the mesh refinement from a breathe and a cough, respectively. An exhale of breathing is visualised with the respective mesh adaptation in figure 21(a) and 21(b). As the particles are ejected, the mesh is automatically adjusted to the particles flowing upwards towards the ceiling. This ensures that the necessary computation for each particle is taken care of. The cough ejects more droplets at a higher magnitude gradually depositing to the desk, creating adaptive grids in the direction of the flow of droplets, as shown in figure 21(c) and 21(d). Utilizing AMR for particle/droplet analysis offers tremendous advantage as the flow of the ejected droplets are not fully known. Refining the mesh manually could lead to less accurate results. The objective of this thesis is to evaluate the airborne droplets behaviour in time and space, making AMR superior for such analysis.

The simulations in this thesis uses an AMR embedding of 3 which offers good results and relatively low computing power. Increasing the embedding to 5 would lead to a slightly better accuracy, but comes with higher computing power demand. The benefit in accuracy might not be significant enough for it to be justified, as explained by the creators of CONVERGE 3.0 [59].

(a) Breathe at 5.6s   (b) Breathe at 7.2s

(c) Cough at 7.6s   (d) Cough at 8s
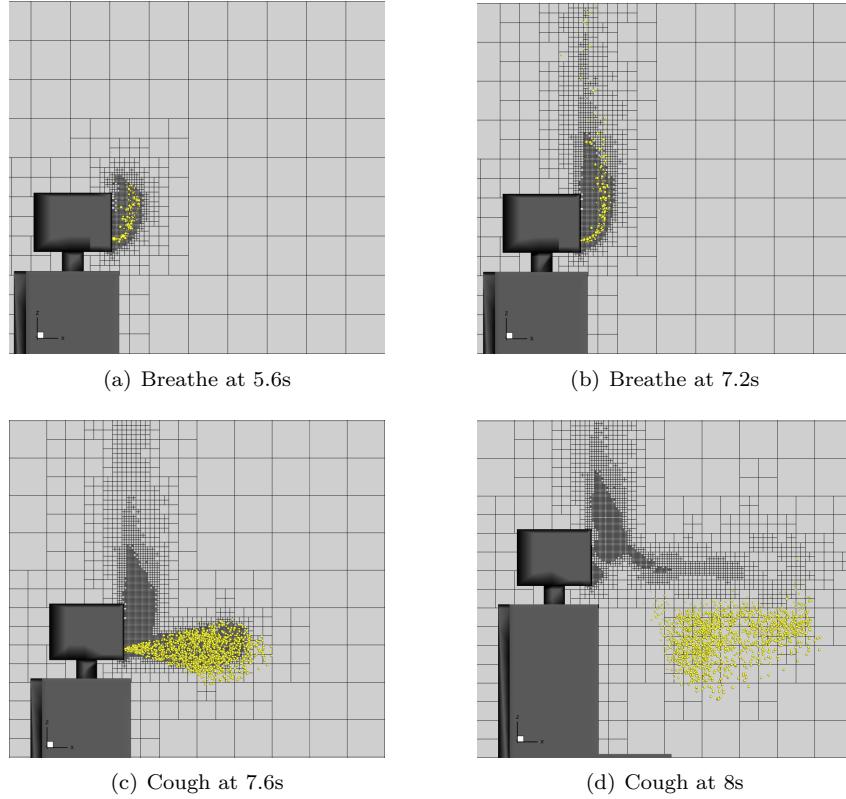
Figure 21: Adaptive mesh refinement for one breathe and one cough

3.3 Dynamics of droplets from breathing, coughing and speaking

The following section highlights the different dynamics of each respiratory event. The factors regarding Lagrangian particles mentioned in section 2.1.4 and 2.2.2 determines the size, form and trajectory of the ejected droplets and it is evident that these are set to the correct value to represent the desired respiratory event realistically.

Figure 22 shows the sequence of breathing at time steps 0.9 s, 8.1 s and 9.3 s. The left figure is a close-up of an exhale, highlighting the particle size distribution with correct scaling and colour to differentiate the droplet sizes. The sizes on the colour-scale are ranging from a radius of 2e-07 μm to 2.4e-06 μm and the results show that there is a high density of particles in the range from r = 1.4e-06 - 2.4e-06 μm and above. At 8.1 s the ejected particles tends to flow upward towards the ceiling because of the thermal plume of each person as well as natural convection. These results show similar characteristics for a breathe as was reported in Bhat et al. [22]. They numerically analyzed the spread of droplets released during coughing, talking and breathing in a conference room. Whether they also applied a temperature boundary for the persons is not clear from their report, yet similar trend of breathing characteristics are found. The right picture is a side-view of the particles at 9.3 s (zy-plane) and the particles are represented as points, not scaled by size, only by colour.

The droplet sizes for the speaking in figure 23 is represented with the same colour-coding and droplet scale
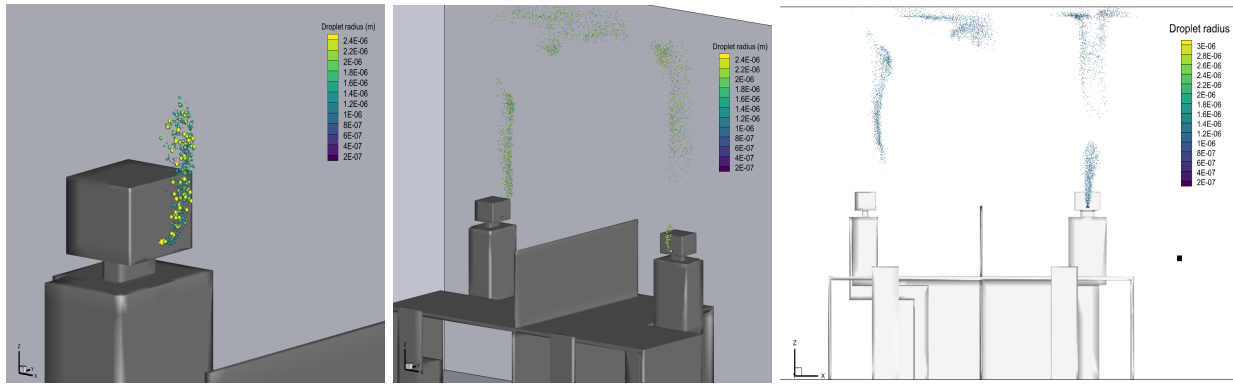
Figure 22: Dynamics of breathing at 0.9s, 8.1s and 9.3s

for the left and middle figure. Here, the velocity is higher (3.9 m/s compared to 1 m/s) resulting in a longer ejection distance. The size of the droplets tend to show more yellow colour, meaning that most of the droplets radius are bigger that 2.4e-06 μm. Similarly, the droplets tends to follow an upwards trajectory towards the ceiling creating a cloud-like shape of droplets above the persons. The right picture is also represented by points, and show that the droplets reach over the partition potentially creating a scenario where droplets containing virus might reach person 2. This risk will increase with a higher magnitude speech or e.g a cough or sneeze.
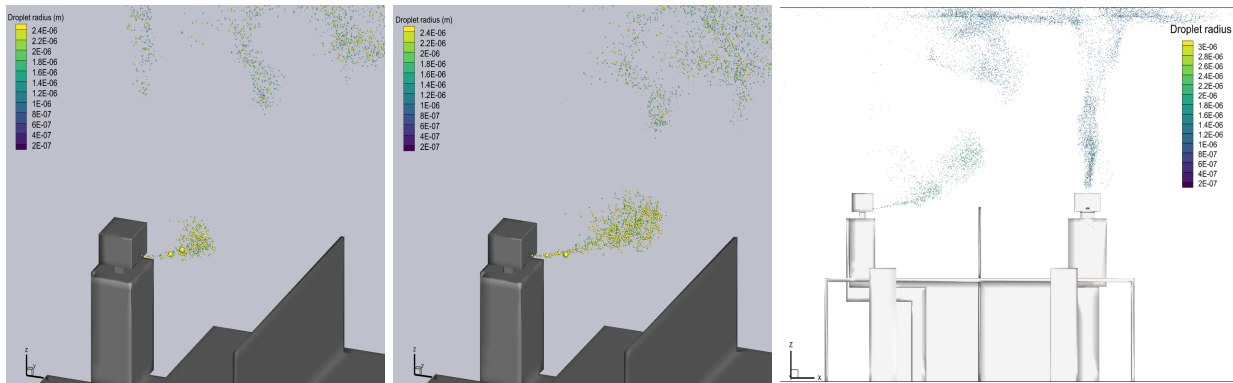
Figure 23: Dynamics of speaking at 10.5s, 12s and 15.5s

The cough in figure 24 is ejected as a ball-shape at the initial stage of the cough at 10.2 s, naturally spreading and breaking up as well as evaporating into smaller sizes over time. The contour scale is ranging from r = 1e-05 μm - 0.0001 μm and scaled by sizes in the left and middle figure. Most of the initial droplet sizes vary between r = 6e-05 μm - 0.0001 μm, in contrast to breathing and speaking which is mostly in low μm sizes. The majority of droplets flows in a ballistic motion depositing to the desk within a short time span. The smallest droplets will evaporate and be dominated by buoyancy forces, flowing in an upwards direction similar to the breathing and speaking, as seen in the right picture in the zy-plane. The right figure also show the distance the larger droplets travels before depositing to the desk, that is 0.66 m, with a height from the mouth to the desk at 0.56 m. Considerations and further analysis must be made whether this is acceptable in terms of social distance recommendations provided by WHO.
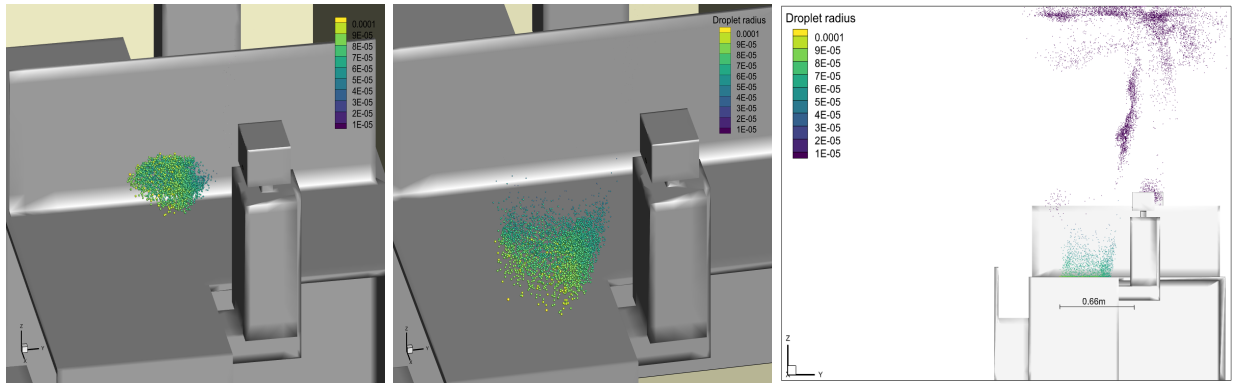
Figure 24: Dynamics of cough at 10.2s, 10.8s and 14.7s

While the dynamics of isolated breathing, coughing and speaking remains fairly predictable as this has been verified by numerous studies in the past, still the challenge of establishing measures of mitigation at a local scale remains. For this particular setup in an office building, as proposed by [21], installing a variation of air curtains in close proximity of the partition could be a possible solution to decrease the risk of the initial particles from a cough or sneeze to reach the other person's desk, as we observe in figure 23. This has not been investigated in the present study and needs more research to be verified.

3.4 Evolution of droplets with MV and DV

As mentioned earlier, the spread of droplets that over time evaporates into airborne aerosols will be governed by the local airflow and buoyancy forces, mainly from the people in this case due to the uniform temperature in the domain. Therefore, the ventilation setup and design as well as ACH is of high interest when discussing measures for mitigation. Both MV and DV strategies with different ACH is investigated.

3.4.1 MV (ACH 1.6)

The evolution of droplets immediately prior to the respiratory sequence is visualized in figure 25 at 30 s, 50 s and 90 s, respectively. The particles are represented by points to ensure a proper visualization, though the sizes are still differentiated by colours. At 30s and 50s most of the particles are larger than r = 1.4e-06 μm but will eventually evaporate into the desired cut-off size as seen at 90 s. The particles flows at a slow pace, initially hovering around the sources. As time goes by, they will spread across most of the room.
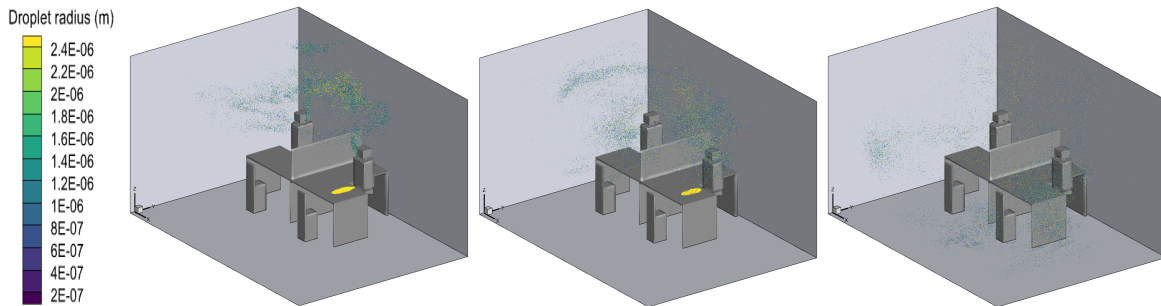
Figure 25: Evolution of droplets at 30s, 50.1s and 90s

At 120 s (see figure 26) a large portion of the particles has deposited to either the floor or the desk, as seen in the left and middle picture. The particles tends to be dominated by the heat sources from the persons, staying afloat above and around them. A portion is also depositing to the floor or floating besides the desk near the floor, more dominated by gravity than buoyancy and air flow. The right picture is seen from above (xy-plane) and shows that the particles are evenly spreading across the room with highest density around the persons. At this time step the evaporation has ceased completely, meaning the cut-off radius is reached for all the particles that remain airborne.
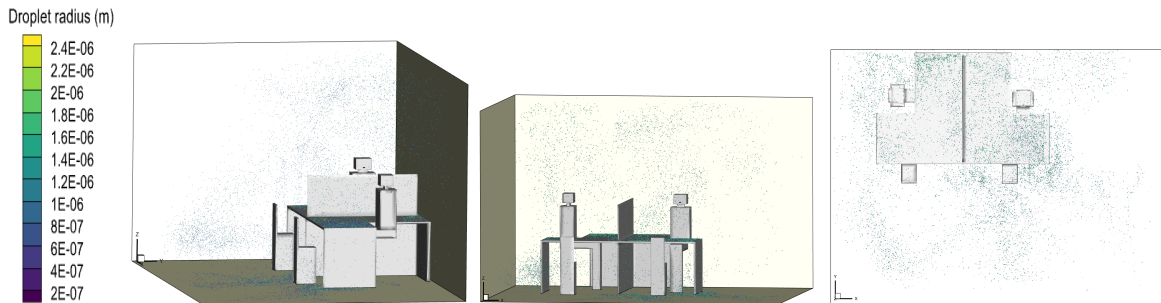
Figure 26: Evolution of droplets at 120s

3.4.2 MV (ACH 3.2)

With a doubling of the air flow rates we see a wider spread of particles across the room, see figure 27. 30 s and 50 s shows similar characteristics as with ACH of 1.6, floating around the persons. The higher air flows creates a greater mixing of the air, and therefore a greater distribution of the particles throughout the domain. Also more particles is seen to deposit to the desk and floor at 90 s.
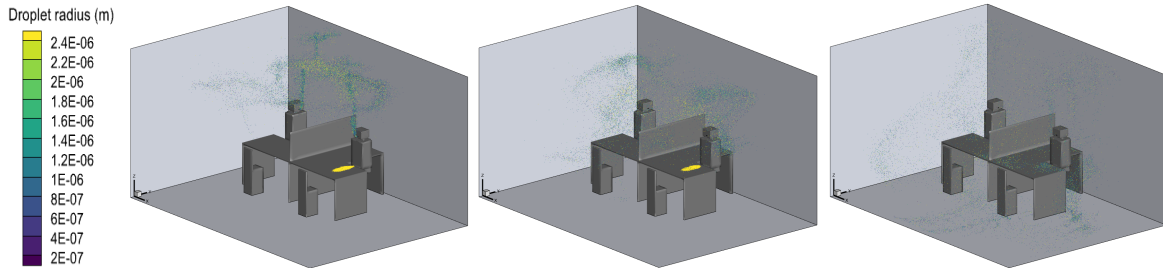
Figure 27: Evolution of droplets at 30s, 50.1s and 90s

As time goes by, a higher concentration of particles is located around and above the persons. We also see a large amount of droplets at the desk and floor. The right picture of figure 28 clearly show a wider spread of particles across the room due to the increased air flow.
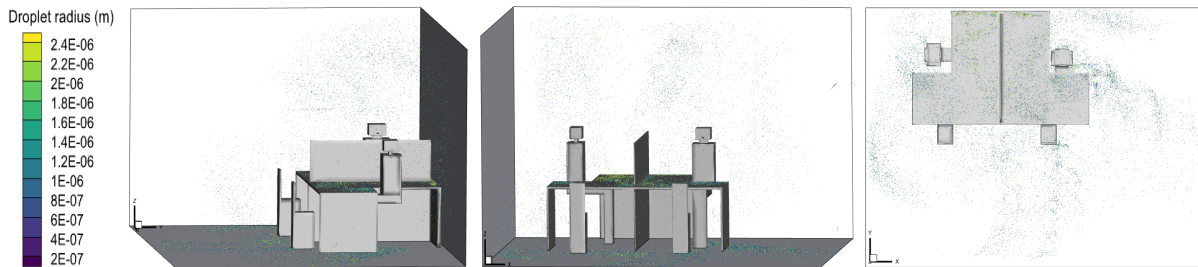
Figure 28: Evolution of droplets at 120s

3.4.3 DV (ACH 1.6)

For the cases with DV the fresh air is supplied near the lower part of the wall at a slow pace. The cold air is then lifted towards the ceiling as it interferes with heat sources in the room, dragging the particles along with it. Figure 29 shows the spread of particles as with MV above. 30 s and 50 s characteristics are fairly similar, much affected by the heating sources from the persons and floating in close connection. A bigger difference is seen from MV to DV at 90 s. Here, the particles are much less spread across the room, and more has deposited to the desk and floor and are no longer airborne. The low ACH from such ventilation system creates a better environment concerning spread of droplets.
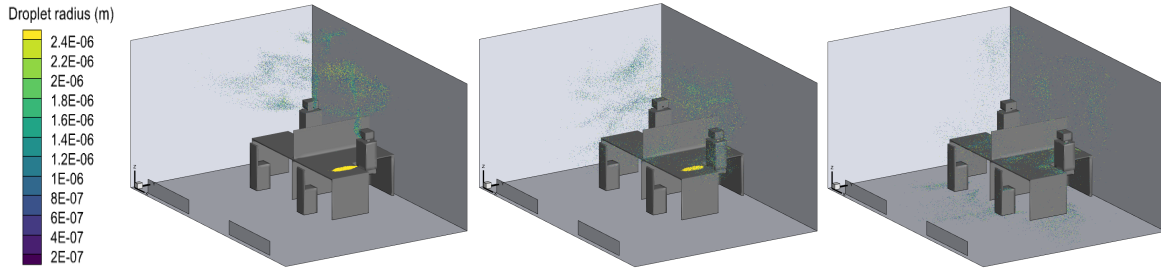
Figure 29: Evolution of droplets at 30s, 50.1s and 90s

At 120 s in figure 30, most of the droplets are in close connection to the persons and there is a significantly lower spread across the room. This is due to the low air velocity decreasing the mixing of air, as desired. The middle picture show that there is a gap between the persons with very few particles. Assumably because of a combination of low air velocity and the fact that particles trajectory are affected by the buoyancy forces from the heat emitted from the persons.
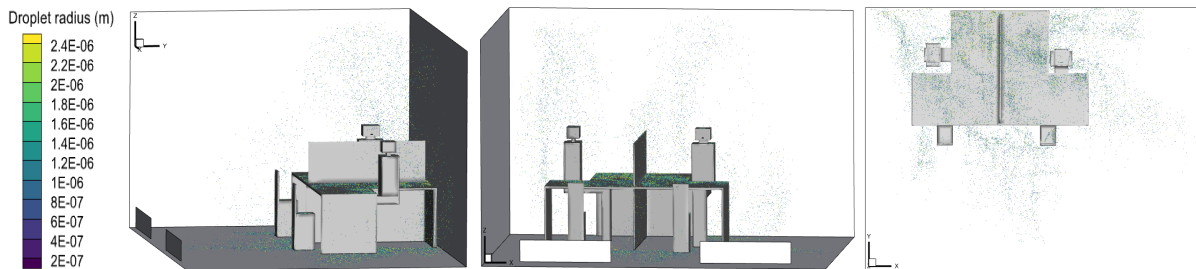
Figure 30: Evolution of droplets at 120s

3.4.4 DV (ACH 3.2)

The results from DV (ACH 3.2) shows fairly similar behaviour of the particles as for DV at ACH 1.6 at 30 s, 50 s and 90 s, seen in figure 31. The difference is more droplets has deposited to the desk and floor at 90 s and the spread is less, but has a few dense areas of particles around the persons and on the desk.
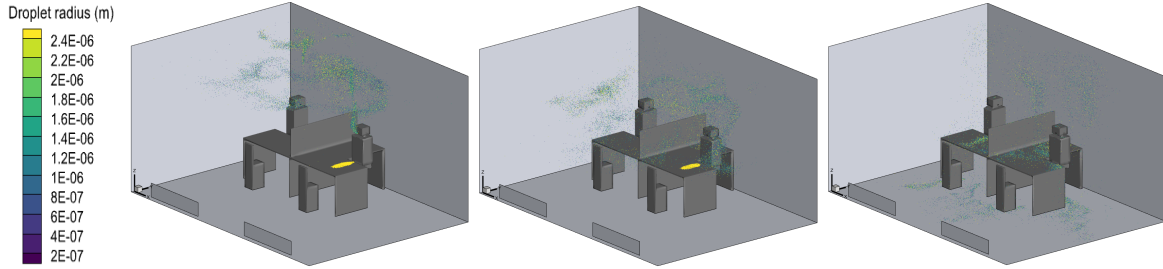
Figure 31: Evolution of droplets at 30s, 50.1s and 90s

Most of the particles will over time keep its position above and around the persons, as shown in the right picture of figure 32. A similar gap between the persons is seen with higher air flow rate as well. In the right picture, the spread is more concentrated around the persons and a few areas of higher particle concentration is observed.
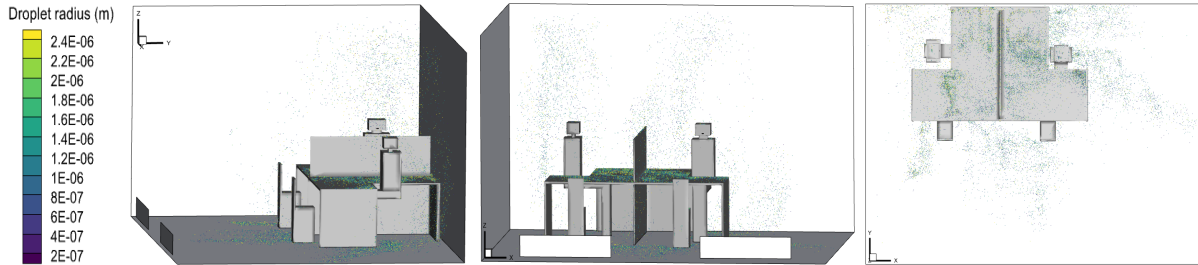
Figure 32: Evolution of droplets at 120s

3.4.5   Wall film accumulation

As seen in figures 26, 28, 30 and 32, with time emerging towards 120 s particles will eventually deposit to nearby surfaces. Figure 33 below illustrates the total amount of mass of the droplets that are deposited to the surfaces, mostly the desk and the floor, within the simulation time of 120 s for cases 1-4 and 30 s for case 5. The results show that most of the droplets are depositing to the desk at 10 s due to the cough instance at that time step. As mentioned, because of the size and mass of such droplets, they fall downwards dominated by gravity. Most of the particles will remain airborne for a period of approximately 50 s, until MV and DV cases starts to deviate. We noticed in our previous section that the DV cases tends to deposit at a higher rate than MV, which is exactly what is shown in the figure below. In the case of motion, case 5, most of the deposited particles is a result of the cough at 10s. The simulation is only 30 s long which is not enough time to get a clear view on the wall film accumulation over time.
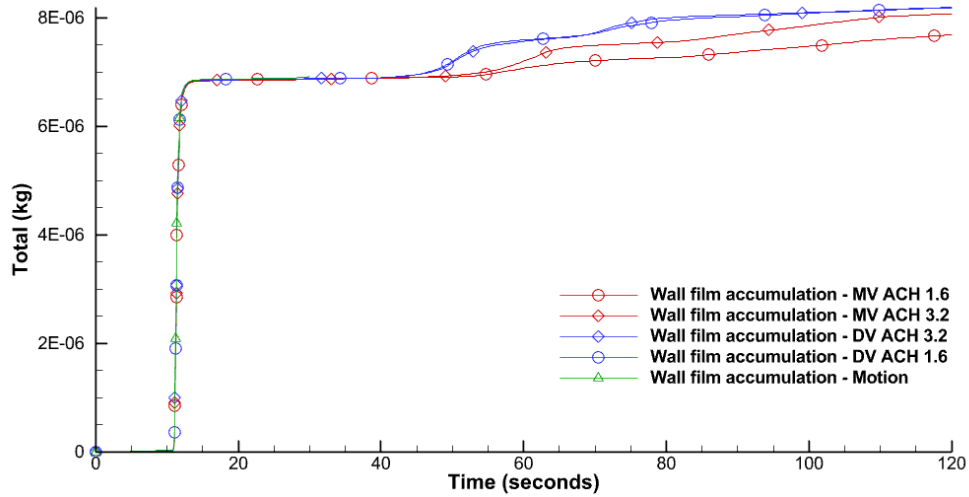
Figure 33: Accumulation of wall film for cases 1-5

3.4.6 Comparison of dispersion of droplets with MV and DV

The following series of figures is visualizing from zx- and zy plane the different behaviour of the dispersed droplets over time at 20 s, 30 s, 50 s, 70 s and 90 s. The particles are represented by points with the same contour as in section 3.4.1, 3.4.2, 3.4.3 and 3.4.4.

(a) MV, ACH 1.6, zx   (b) MV, ACH 3.2, zx   (c) DV, ACH 1.6, zx   (d) DV, ACH 3.2, zx

(e) MV, ACH 1.6, zy   (f) MV, ACH 3.2, zy   (g) DV, ACH 1.6, zy   (h) DV, ACH 3.2, zy
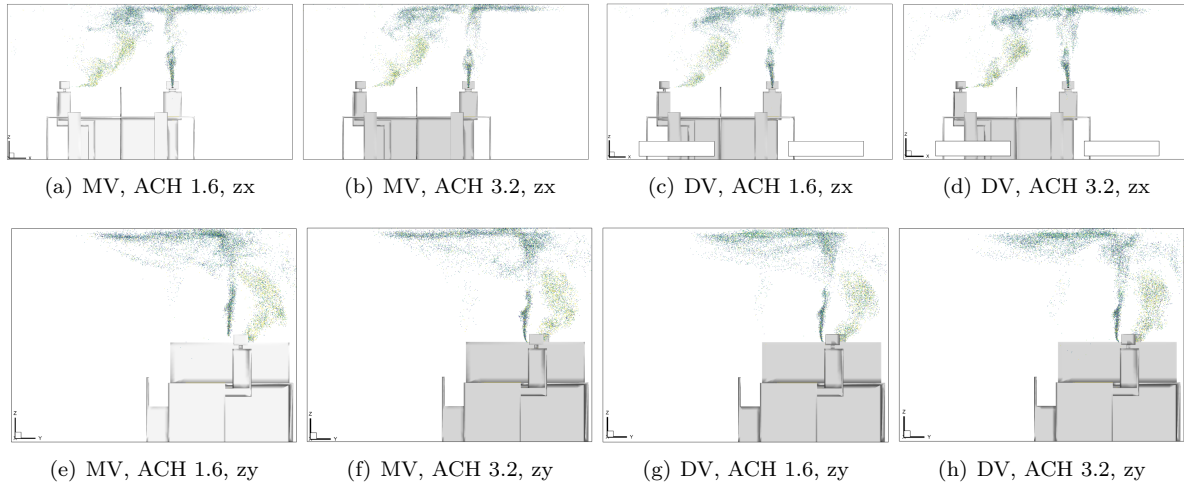
Figure 34: Comparison of droplet dispersion due to different ventilation strategy at 20s

At 20 s, as seen in figure 34 no significant differences are occurring as it is still at an early stage. Differences starts appearing at 30 s (figure 35) especially in the zy-plane, where MV is showing a wider spread of the particles at ceiling level towards the negative y-direction. Both DV cases has a smaller spread in the y direction in comparison. DV with ACH 3.2 shows the least spread in all directions.

(a) MV, ACH 1.6, zx   (b) MV, 3.2 ACH, zx   (c) DV, ACH 1.6, zx   (d) DV, ACH 3.2, zx

(e) MV, ACH 1.6, zy   (f) MV, ACH 3.2, zy   (g) DV, ACH 1.6, zy   (h) DV, ACH 3.2, zy
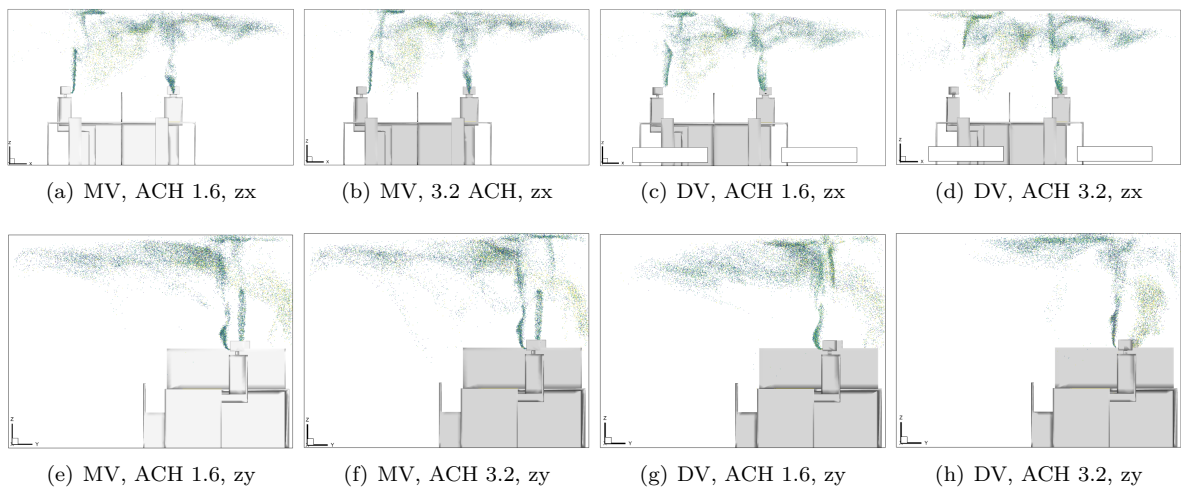
Figure 35: Comparison of droplet dispersion due to different ventilation strategy at 30s

Continuing with the 50 s time snaps in figure 36. For the MV cases in both zy and zx planes the particles tend to spread along a bigger area at a higher z-value, closer to the ceiling. Whereas both DV cases has a larger portion of particles around the breathing zone. MV with ACH 1.6 forms a cloud covering most of the upper half of the room as seen in figure 36(a). As for both DV cases, most of the particles are rather stationary around the persons.

(a) MV, ACH 1.6, zx   (b) MV, 3.2 ACH, zx   (c) DV, ACH 1.6, zx   (d) DV, ACH 3.2, zx

(e) MV, ACH 1.6, zy   (f) MV, ACH 3.2, zy   (g) DV, ACH 1.6, zy   (h) DV, ACH 3.2, zy
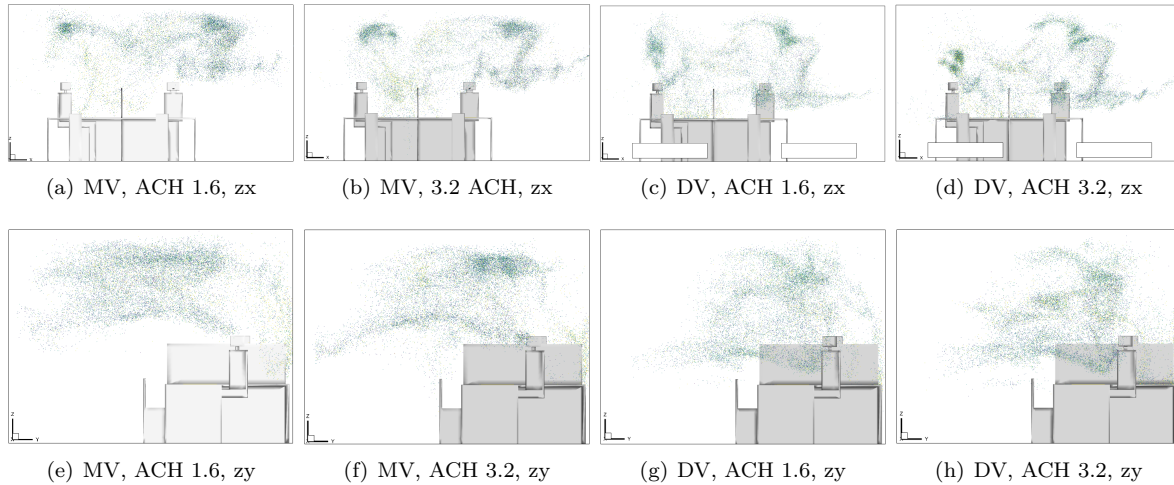
Figure 36: Comparison of droplet dispersion due to different ventilation strategy at 50s

As the time emerges towards 70 s in figure 37, the particles for both MV cases falls downwards creating a dense area in the breathing zone, whereas the DV cases are more affected by the heat from the persons and less by the air flow, and forming a vertical cloud of particles above the persons. Also, more particles have deposited to either the desk or the floor, as mentioned above.

(a) MV, ACH 1.6, zx   (b) MV, 3.2 ACH, zx   (c) DV, ACH 1.6, zx   (d) DV, ACH 3.2, zx

(e) MV, ACH 1.6, zy   (f) MV, ACH 3.2, zy   (g) DV, ACH 1.6, zy   (h) DV, ACH 3.2, zy
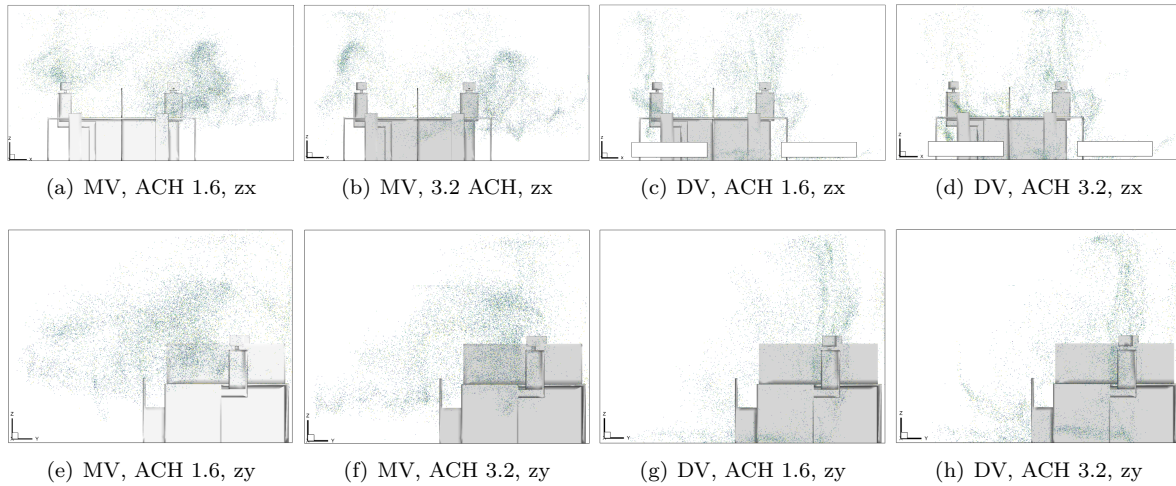
Figure 37: Comparison of droplet dispersion due to different ventilation strategy at 70s

At 90 s the MV cases show higher concentration around the persons towards the ground, the spread is significantly higher compared to DV cases. Both DV cases has less airborne particles mainly concentrated above the persons, seen in figure 38.

(a) MV, ACH 1.6, zx   (b) MV, 3.2 ACH, zx   (c) DV, ACH 1.6, zx   (d) DV, ACH 3.2, zx

(e) MV, ACH 1.6, zy   (f) MV, ACH 3.2, zy   (g) DV, ACH 1.6, zy   (h) DV, ACH 3.2, zy
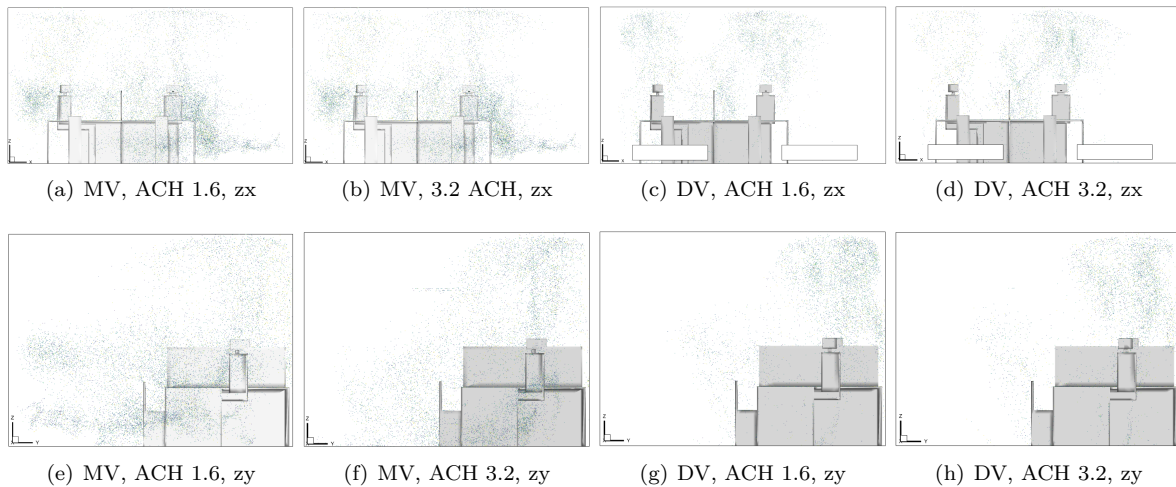
Figure 38: Comparison of droplet dispersion due to different ventilation strategy at 90s

As we noticed in the above cases, the MV increases the mix of air in the room causing the particles to spread across a larger area, while DV causes a calm dispersion of the droplets that either falls to the ground or hovers around the heating plumes. Very few particles are seen to be removed through the duct and does not follow trajectories of the air flow to the degree as we desire. A part of the reason for this is assumed to be because of the lack of proper stratification in the room, which is essential to constructing a proper DV strategy for a room. The particles have a higher temperature than the room initially and are also being influenced by the thermal plumes of the people, which causes them to rise due to buoyancy. The temperature

of the particles will gradually decline until they reach room temperature, and buoyancy will have little effect. As a result, gravity has a stronger influence on the particles than buoyancy and local air movement, limiting droplet extraction. The denser areas of particles that are observed in the results above could be a result of improper dispersion air, creating local pockets of air which is not resolved. This needs further analysis.

Other important aspects of choosing correct ventilation strategy has to be considered alongside particle dispersion and extraction. MV and DV both have pros and cons in its natural design. MV is rather simple and needs less consideration in terms of room layout and usage. DV on the other hand is more complex as the design requires a placement of the supply air near the floor, meaning that there are more requirements to meet in order to ensure proper airflow. The layout of the room must be done such that the supply air is not covered, and the usage of the room is more important to consider. Similar to both cases, an increase of ACH shows to slightly decrease the dispersion of droplets. While this is a positive result in terms of our objective, increasing the ACH will lead to other issues such as draft, causing an unsatisfying indoor environment.

3.5   Dynamics of droplets emitted from a moving person

The dispersion of viral droplets emitted from a person in motion plays a key role in the transmission of infectious viruses, as it is a highly relevant daily activity for all people. Understanding the spread of droplets resulting from such event and how velocity affects the dispersion lacks a complete understanding.

The illustration in figure 39 below illustrates a timeline of a speech event from 21.3 s to 27.0 s of a total simulation of 30 s with respiratory sequence 2. The initial speech-droplets ejected at 22.6 s shows that different-sized particles tends to flow upwards and above the head as a result of the velocity field created by the motion. The bigger sizes will evaporate rather quickly and follow the similar trajectory, as seen at 23.7 s. Turbulent eddies created behind the person in head height will dominate the dispersion of the droplets, as seen in 24.9 s. The eddies are also visualized in figure 40 below. After a short inhale of 0.8 s, the speech continues at 25.8 - 27.0 s creating a similar particle behaviour. The person is walking at a relatively slow pace at 0.5 m/s and it is assumed that a higher velocity would create more significant dispersion of the droplets and turbulent eddies of higher magnitude. Another observation we notice is that a portion of the ejected particles will remain at the location where they were injected, here measured to 2.3 m in shoulder height behind the person at 27.0 s. This could potentially cause a risk if someone walks behind an infected person. Li et al. [24] presented similar findings on the dispersion of droplets from a cough, stating that a cloud of particles locates around and below waist-height 2s after the cough. Their model includes a man walking in 1.2 - 1.8 m/s as well as a different ventilation setup and flow rates, which could be a reason for the height difference of the dispersed droplets.
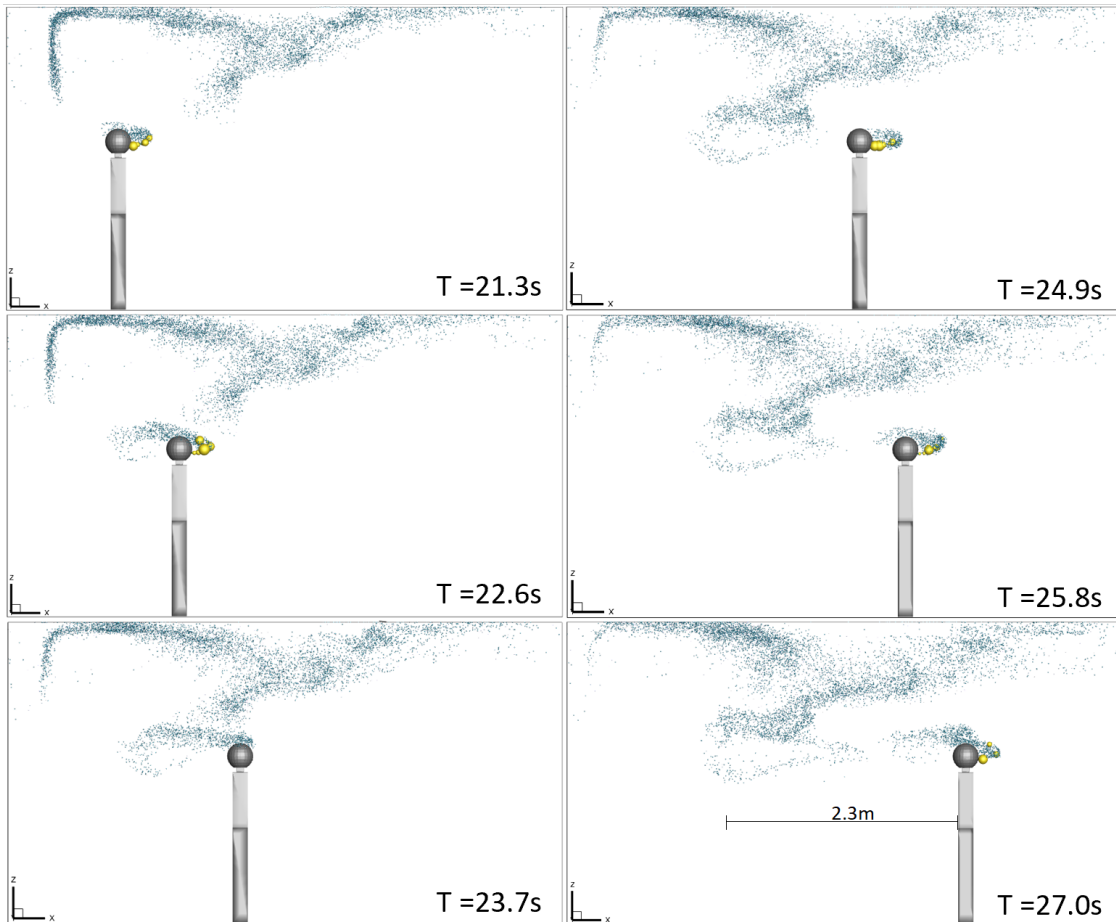
Figure 39: Dispersion of speech-generated droplets from a walking person

figure 40 visualizes the velocity and flow field caused by human motion of 0.5 m/s at different time steps from 21.3 - 27.9 s. The flow field is represented by white streamlines and the velocity in represented by a contour scale from 0.04 m/s - 2 m/s. As the person starts walking, smaller turbulent eddies starts forming above the head at 22.2 s and 23.4 s. The initial eddies gets larger as the person moves, forming an area towards the ceiling with lower magnitude eddies of bigger size, as seen at 24.2 - 27.9 s. The person's movement creates a low-pressure zone behind him, which causes the streamlines to form an organized flow along the walking path towards positive x-direction. The eddies behind the head disrupt the structured flow field, forcing the particles downward and forming a "C" shape, as shown in figure 39 at 23.7 s. Some particles will also be caught up in the airflow caused by the human motion and be dragged along the walking direction.
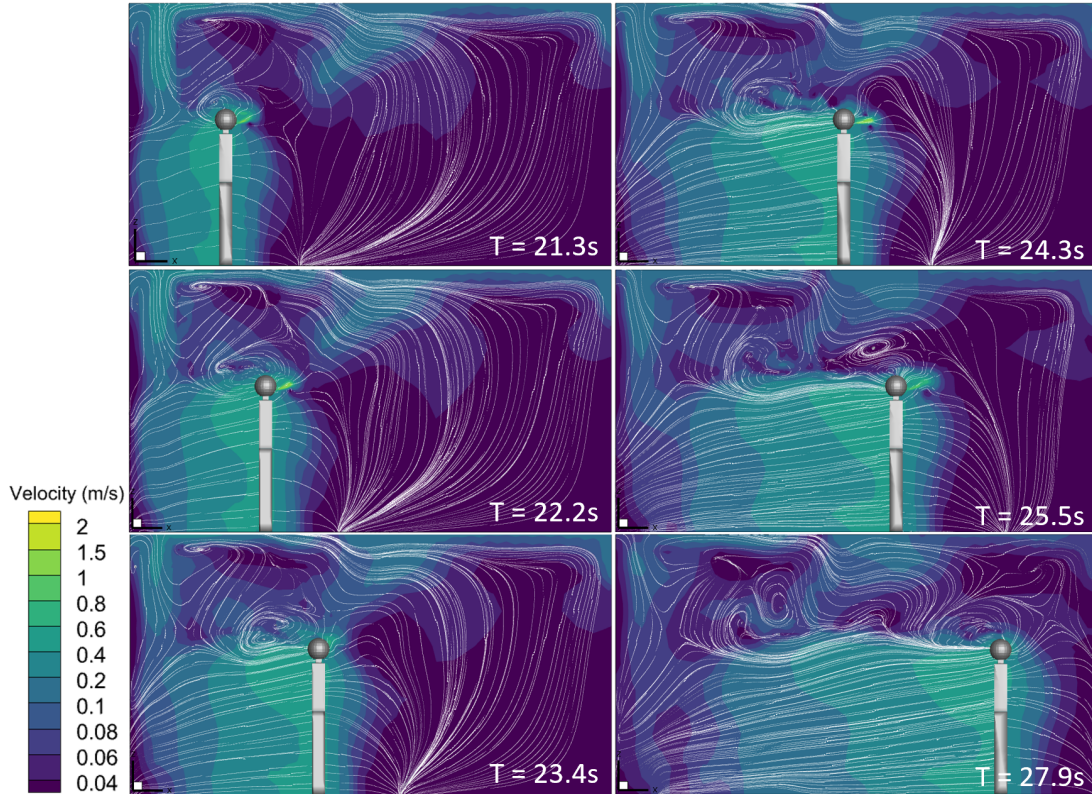
Figure 40: Contour plot of velocity and streamlines caused by human motion

3.6 Evolution of particles from a walking person

Figure 41 and 42 show the dispersion of droplets from case 5 at different time steps. The initial particles behaves in a similar manner as the cases 1-4 with the difference in amount of particles injected to the domain due the extra person. Compared to case 1 in figure 35(a) (which has similar ventilation setup), the particles are spreading significantly more. Similar to examples 1-4, the particles ejected by persons 1 and 2 will be dominated by their respective heat plumes and will remain in close proximity, but because person 3 is not stationary, the particles ejected will disperse more widely around the room. The majority of the particles are still airborne after 30 s.
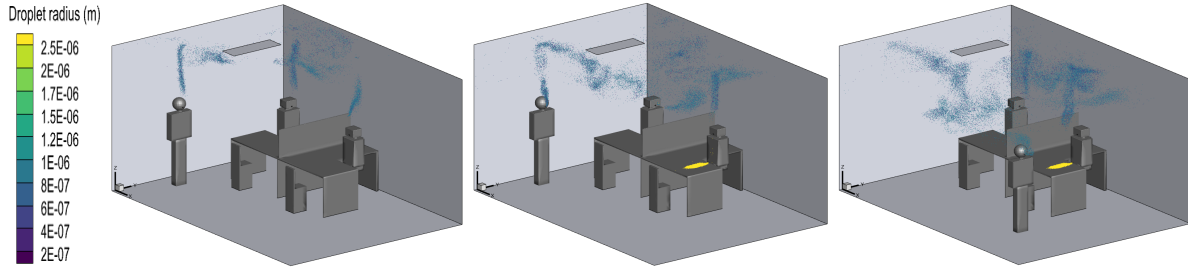
Figure 41: Evolution of droplets at 9s, 17.2s and 27s
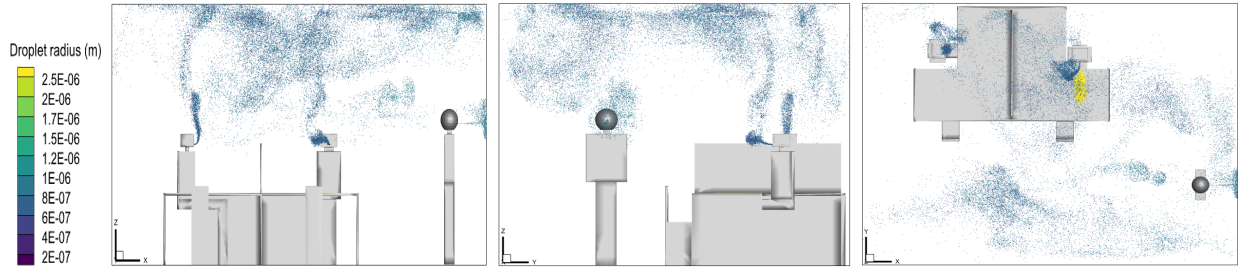
Figure 42: Evolution of droplets at 30 s in zx, zy and zy plane

3.7 Droplet size distribution

The resulting size distributions for each case is presented in histograms below at three different time steps, 0.9 s, 10.2 s and 120 s. 0.9s shown in figure 43 represents the distribution from a breathing only and we notice that the cases are fairly similar with the biggest portion of droplets around 1 μm. The distributions are following a log-normal shape distribution with the majority of particles ranging from 0.3 μm - 2.6 μm. A minor portion of droplets are between 3-10 μm, but is not visible from the histograms.
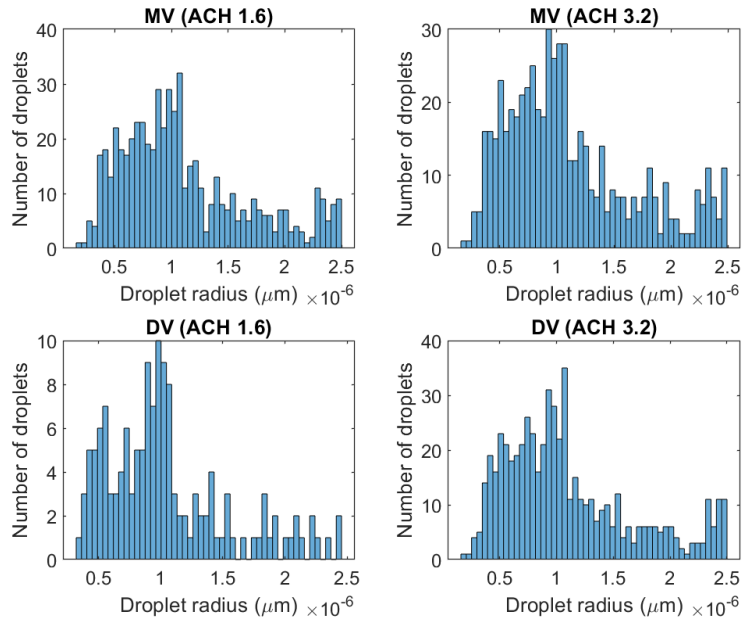
Figure 43: Droplet size distribution at t = 0.9s

At 10.2s in figure 44, we see a distribution of only the droplets that are larger than 2.5 μm, resulting mostly from the cough. This is because the already ejected droplets in sizes around 1 μm represents the largest portion of droplets in the domain at 10.2 s, and would disrupt the visualization of the larger droplets from the cough.
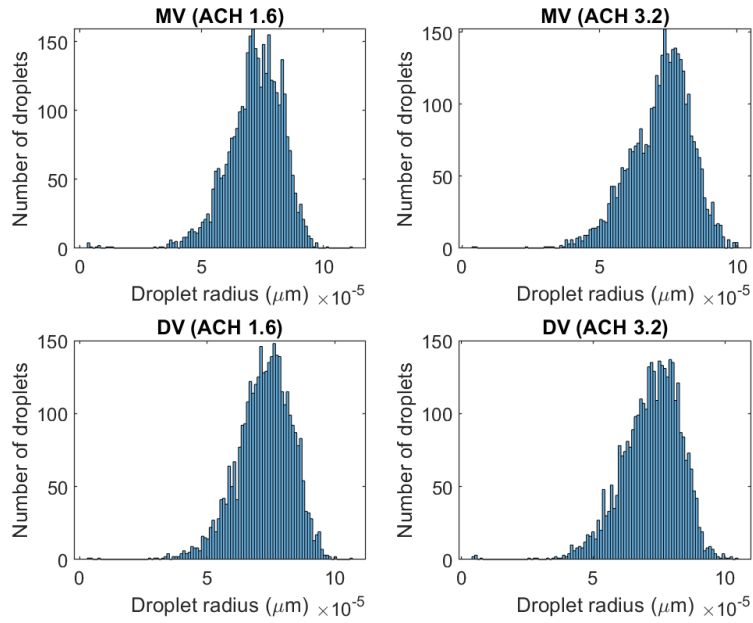
Figure 44: Droplet size distribution of coughed droplets at t = 10.2s

We also observe in figure 45 at 120 s that all of the injected droplets have evaporated to a maximum of 2.5 μm with the majority of droplets being in the size range around 1 μm. Breathing and speaking makes up the greatest portion of the injected droplets, and since the initial size of these droplets is within a size range of 0.3-15 μm as stated in the section 2.2.2, it is a reasonable distribution of droplets.
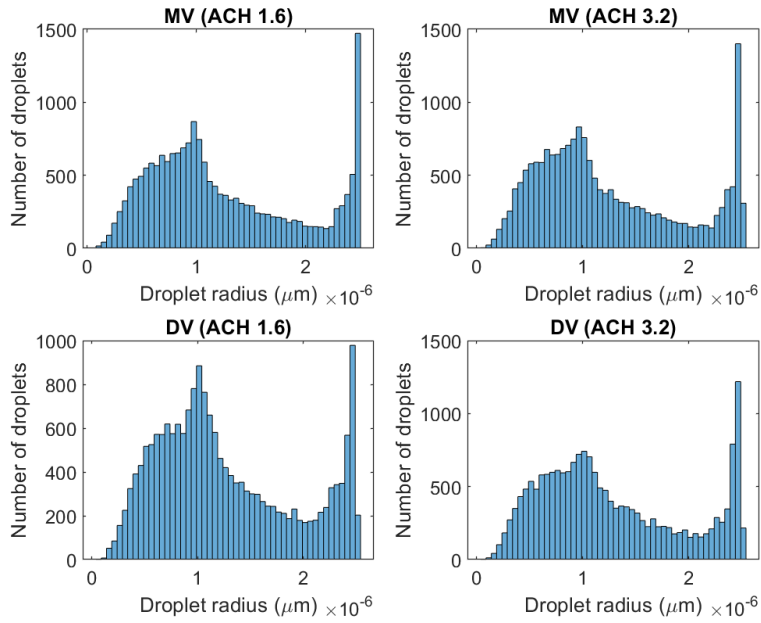
Figure 45: Droplet size distribution at t = 120s

In addition, The change in SMD is visualized in figure 46 for each case, showing how the sizes changes over time as the respiratory sequence emerges. The initial SMD is approximately 1 μm from 0 - 10 s as a result of breathing. At 10 s the cough is initiating, causing a steep spike in the SMD from 1 - 55 μm. These droplets are rapidly evaporating until it stabilizes at approximately 2.5 μm.
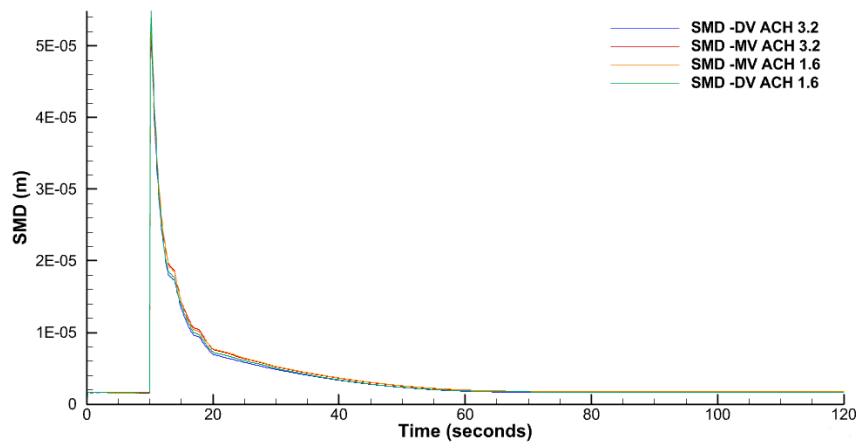
Figure 46: Evolution of SMD of the droplets

3.8 Memory usage

In figure 47 below a comparison of memory usage per seconds for each case is visualized. Cases 1-4 are showing similar results with an initial cost of approximately 2.6e04 MB/s and are more or less stabilizing after 30 s at 3e04 MB/s. Case 5 has an initial memory usage of approximately 12e04 MB/s with a linear increase over time until the end of the simulation at 30 s. Case five involves one additional person and one might assume that would result in a higher cost than cases 1-4. The difference between cases 1-4 and case 5 is that the base grid is increased to 0.2 instead of 0.15 in the in case 5. This clearly shows that creating mesh plays a huge role in terms of energy usage and that simulations must be set up with this in mind. In times of global warming, reducing CO_2 emission and electricity use is an important objective all around the world. Utilizing methods that takes this into account should be a priority within computing as well. Methods like AMR that can assist refining the grids in areas where we have the greatest change of variable and reduce it where it is not needed is key for future numerical simulations.
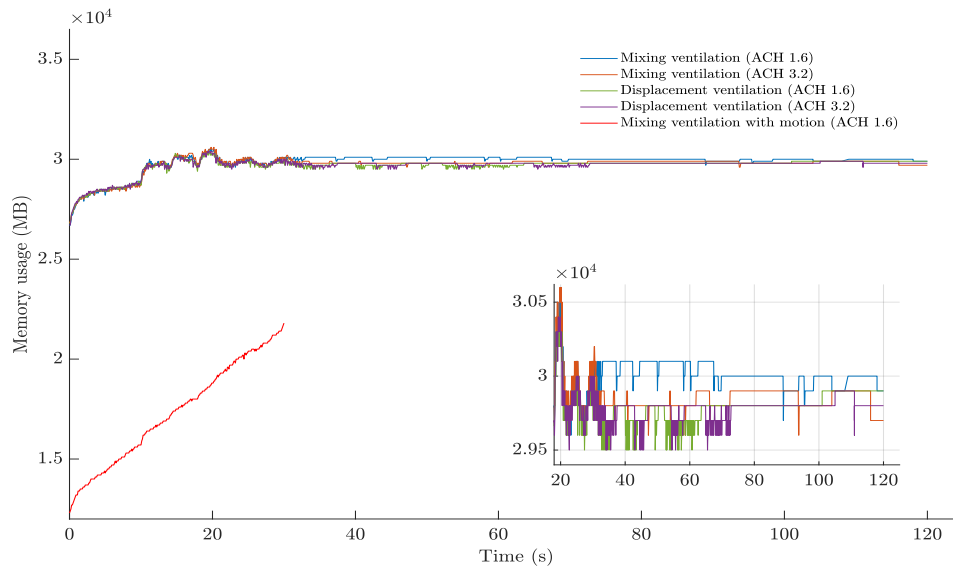
Figure 47: Memory usage for cases 1-5

4   Conclusion

In this study, a realistic approach to the dispersion of particles from human breathing, coughing and speaking in a small double office has been investigated with MV and DV, involving static human beings as well as human motion. The multi-component compressible dispersion media is solved with Eulerian approach and the dispersed phase is resolved by Lagrangian approach utilizing a FVM based efficient 3D multiphase flow solver with AMR. A user defined function is implemented to all the simulations to cease evaporation of particles smaller than a diameter of 5 μm, as numerous studies has reported that particles of such sizes will remain airborne. First, the dynamics of breathing, coughing and speaking is analysed with static human beings, showing the complex flow, patterns and evolution of initial respiratory droplets from different events. The preliminary results are shown to be in accordance with existing literature. Further analysis is then conducted on the evolution and dispersion of the ejected particles with different ventilation strategies and ACH for a total of 120 s. Lastly, human motion is integrated to the MV model to observe the behaviour of particles affected by an additional flow of higher magnitude.

The efficacy of the present method is demonstrated throughout the cases 1-5 showing that the combination of an advanced flow solver and AMR resolves the injected particles' trajectory within the domain. Comparison of MV and DV (cases 1-4) show similar dispersion characteristics at first, but starts deviating as time emerges towards 30 s. MV established a more mixed air flow, causing the particles to disperse at a higher rate throughout the room, whereas DV characteristics show that the particles are less affected by the air flow and their trajectories tends to be dominated by heat plumes of the persons, resulting in a cloud of particles around and above the persons. Both MV and DV with higher ACH results in less dispersion throughout the room, with more particles being accumulated in the wall film, mostly the floor and desk. As for case 5 we noticed that some particles remains in a rather fixed position at shoulder height and some will be dragged along with the person due to a low pressure field caused by the human motion. The present work establishes a basis of understanding on dispersion of respiratory particles and airborne transmission in relation to different ventilation setups as well as human motion. We implemented a novel approach to resolve airborne droplet dynamics with UDF in combination with human motion, which to the best of our knowledge has not been reported in earlier studies.

We see a clear trend that DV limits the dispersion of respiratory particles with both high and low ACH, compared to MV, which is similar to the findings in the review of Lipinski et al. [20], as mentioned in section 1.1. As for the removal of particles, with the present conditions it is not decisive to conclude on which ventilation strategy is preferred. Further investigation are needed to conclude on the efficiency of these systems. Some suggestions based on the limitations of the present study includes ensuring proper stratification for each domain to gain a more realistic perspective on the dispersion of particles, and further investigation with quantitative risk assessment of respiratory droplets from an infected person. As DV is usually a preferred strategy in buildings with taller spaces, such as theatres, conference rooms and cinemas, we suggests that the present method should be used in such a settings involving multiple people with a realistic human body model and different ventilation strategies.

References

[1] World Health Organization. *Weekly epidemiological update on COVID-19 - 12 April 2022*. Published: 4-12-2021.

[2] U.s Environmental protection agency. *Report to Congress on Indoor Air Quality: Volume II - Assessment and Control of Indoor Air Pollution*. Published: 1989.

[3] Centers for Disease Control and Prevention. *Scientific Brief: SARS-CoV-2 Transmission*. Published: 5-7-2021.

[4] Renyi Zhang et al. "Identifying airborne transmission as the dominant route for the spread of COVID-19". In: *Proceedings of the National Academy of Sciences* 117.26 (2020), pp. 14857–14863.

[5] Statista. *Infection rates of viruses involved in outbreaks worldwide as of 2020*. Published: 8-24-2020.

[6] World Health Organization. *Infection prevention and control of epidemic-and pandemic prone acute respiratory infections in health care*. Published: 2014.

[7] Talib Dbouk and Dimitris Drikakis. "On coughing and airborne droplet transmission to humans". In: *Physics of Fluids* 32.5 (2020), p. 053310.

[8] Bert Blocken et al. "Ventilation and air cleaning to limit aerosol particle concentrations in a gym during the COVID-19 pandemic". In: *Building and Environment* 193 (2021), p. 107659.

[9] Talib Dbouk and Dimitris Drikakis. "On respiratory droplets and face masks". In: *Physics of Fluids* 32.6 (2020), p. 063303.

[10] Talib Dbouk and Dimitris Drikakis. "On airborne virus transmission in elevators and confined spaces". In: *Physics of Fluids* 33.1 (2021), p. 011905.

[11] Paulsen Patrick. "Analysis of human cough in confined spaces: a numerical study". Master's Thesis. Oslo: Institutt for bygg- og energiteknikk, Oslo Metropolitan University, 2021. URL: https://hdl.handle.net/11250/2772566.

[12] William G Lindsley et al. "Viable influenza A virus in airborne particles from human coughs". In: *Journal of occupational and environmental hygiene* 12.2 (2015), pp. 107–113.

[13] Jing Yan et al. "Infectious virus in exhaled breath of symptomatic seasonal influenza cases from a college community". In: *Proceedings of the National Academy of Sciences* 115.5 (2018), pp. 1081–1086.

[14] Lidia Morawska and Donald K Milton. "It is time to address airborne transmission of coronavirus disease 2019 (COVID-19)". In: *Clinical Infectious Diseases* 71.9 (2020), pp. 2311–2313.

[15] Lidia Morawska and Junji Cao. "Airborne transmission of SARS-CoV-2: The world should face the reality". In: *Environment international* 139 (2020), p. 105730.

[16] Clifford K Ho. "Modelling airborne transmission and ventilation impacts of a COVID-19 outbreak in a restaurant in Guangzhou, China". In: *International Journal of Computational Fluid Dynamics* (2021), pp. 1–19.

[17] Clifford K Ho. "Modeling airborne pathogen transport and transmission risks of SARS-CoV-2". In: *Applied Mathematical Modelling* 95 (2021), pp. 297–319.

[18] Ville Vuorinen et al. "Modelling aerosol transport and virus exposure with numerical simulations in relation to SARS-CoV-2 transmission by inhalation indoors". In: *Safety Science* 130 (2020), p. 104866.

[19] Siyao Shao et al. "Risk assessment of airborne transmission of COVID-19 by asymptomatic individuals under different practical settings". In: *Journal of aerosol science* 151 (2021), p. 105661.

[20] Tom Lipinski et al. "Review of ventilation strategies to reduce the risk of disease transmission in high occupancy buildings". In: *International Journal of Thermofluids* 7 (2020), p. 100045.

[21]   Mariam et al. "CFD simulation of the airborne transmission of COVID-19 vectors emitted during respiratory mechanisms: Revisiting the concept of safe distance". In: *ACS omega* 6.26 (2021), pp. 16876–16889.

[22]   Sourabh P Bhat et al. "Modeling and simulation of the potential indoor airborne transmission of SARS-CoV-2 virus through respiratory droplets". In: *Physics of Fluids* 34.3 (2022), p. 031909.

[23]   Zhaobin Li et al. "Effects of slope and speed of escalator on the dispersion of cough-generated droplets from a passenger". In: *Physics of Fluids* 33.4 (2021), p. 041701.

[24]   Zhaobin Li et al. "Effects of space sizes on the dispersion of cough-generated droplets from a walking person". In: *Physics of Fluids* 32.12 (2020), p. 121705.

[25]   Convergent Science. *CONVERGE MANUAL 3.0*. Published: 11-19-2021.

[26]   W Malalasekera H.K Versteeg. *An introduction to computational fluid dynamics. The finite volume method*. Pearson, 2007.

[27]   Osborne Reynolds. "IV. On the dynamical theory of incompressible viscous fluids and the determination of the criterion". In: *Philosophical transactions of the royal society of london.(a.)* 186 (1895), pp. 123–164.

[28]   W Malalasekera H.K Versteeg. *An introduction to computational fluid dynamics. The finite volume method*. Pearson, 2007, pp. 66–91.

[29]   Hatef Seyyedvalilu. *Difference between standard and realizable k-epsilon model?* Oct. 2018. URL: `https://www.researchgate.net/post/Difference-between-standard-and-realizable-k-epsilon-model/5bd21ce04921ee877d74a6da/citation/download`.

[30]   Convergent Science. *CONVERGE MANUAL 3.0*. Published: 11-19-2021.

[31]   Raul Raghav. *Near wall treatment*. Published: 11-19-2021.

[32]   the free encyclopedia Wikipedia. *Law of the wall*. Online, accessed: 3-22-2022.

[33]   Convergent Science. *CONVERGE MANUAL 3.0*. Published: 11-19-2021.

[34]   W Malalasekera H.K Versteeg. *An introduction to computational fluid dynamics. The finite volume method*. Pearson, 2007, pp. 1–4.

[35]   inc Tecplot. *CFD visualisation and analysis tools*. Accessed: 3-24-2022.

[36]   W Malalasekera H.K Versteeg. *An introduction to computational fluid dynamics. The finite volume method*. Pearson, 2007, p. 179.

[37]   Anastasia Churazova. *How to optimize displacement ventilation design using CFD*. Published: 10-12-2020.

[38]   Direktoratet for byggkvalitet. *Byggteknisk Forskrift 17*. Reviewed: 9-15-2017.

[39]   MD Melissa Conrad Stöppler. *Medical Definition of Body surface area*. Reviewed: 3-29-2021.

[40]   Gen Pei, Mary Taylor, and Donghyun Rim. "Human exposure to respiratory aerosols in a ventilated room: Effects of ventilation condition, emission mode, and social distancing". In: *Sustainable Cities and Society* 73 (2021), p. 103090.

[41]   Jitendra K Gupta, C-H Lin, and Q Chen. "Flow dynamics and characterization of a cough". In: *Indoor air* 19.6 (2009), pp. 517–525.

[42]   NP Gao and JL Niu. "CFD study of the thermal environment around a human body: a review". In: *Indoor and built environment* 14.1 (2005), pp. 5–16.

[43]   BE Scharfman et al. "Visualization of sneeze ejecta: steps of fluid fragmentation leading to respiratory droplets". In: *Experiments in Fluids* 57.2 (2016), pp. 1–9.

[44] Christopher Yu Hang Chao et al. "Characterization of expiration air jets and droplet size distributions immediately at the mouth opening". In: *Journal of aerosol science* 40.2 (2009), pp. 122–133.

[45] Shengwei Zhu, Shinsuke Kato, and Jeong-Hoon Yang. "Study on transport characteristics of saliva droplets produced by coughing in a calm indoor environment". In: *Building and environment* 41.12 (2006), pp. 1691–1702.

[46] X Xie et al. "How far droplets can move in indoor environments–revisiting the Wells evaporation-falling curve." In: *Indoor air* 17.3 (2007), pp. 211–225.

[47] Jitendra K Gupta, Chao-Hsin Lin, and Qingyan Chen. "Characterizing exhaled airflow from breathing and talking". In: *Indoor air* 20.1 (2010), pp. 31–39.

[48] Convergent Science. *CONVERGE MANUAL 3.0*. Published: 11-19-2021.

[49] Xiaojian Xie et al. "Exhaled droplets due to talking and coughing". In: *Journal of the Royal Society Interface* 6.suppl_6 (2009), S703–S714.

[50] NN Peng, KW Chow, and CH Liu. "Computational study on the transmission of the SARS-CoV-2 virus through aerosol in an elevator cabin: Effect of the ventilation system". In: *Physics of Fluids* 33.10 (2021), p. 103325.

[51] JP Duguid. "The size and the duration of air-carriage of respiratory droplets and droplet-nuclei". In: *Epidemiology & Infection* 44.6 (1946), pp. 471–479.

[52] Barry J. Azzopardi. *Sauter mean diameter*. Published: 2-2-2011.

[53] LJGR Morawska et al. "Size distribution and sites of origin of droplets expelled from the human respiratory tract during expiratory activities". In: *Journal of aerosol science* 40.3 (2009), pp. 256–269.

[54] Valentyn Stadnytskyi et al. "The airborne lifetime of small speech droplets and their potential importance in SARS-CoV-2 transmission". In: *Proceedings of the National Academy of Sciences* 117.22 (2020), pp. 11875–11877.

[55] Sima Asadi et al. *The coronavirus pandemic and aerosols: Does COVID-19 transmit via expiratory particles?* 2020.

[56] Kimberly A Prather, Chia C Wang, and Robert T Schooley. "Reducing transmission of SARS-CoV-2". In: *Science* 368.6498 (2020), pp. 1422–1424.

[57] Sigma2 AS. *Sigma2 — the national provider of e-infrastructure.* `https://www.sigma2.no/`.

[58] Convergent Science. *CONVERGE 3.0 UDF MANUAL*. Published: 11-19-2021.

[59] Convergent Science. *CONVERGE CFD SOFTWARE.* `https://hub.convergecfd.com/training`.

Appendices

A   Nozzle diameter

	Nozzle diameter
velocity (m/s)	1
mass (kg)	0.000000066
dt_breath (s)	5
rho (kg/m3)	1019.32
d=	=ROT((C4*4)/(C6*C3*C5*3.14))

Figure 48: Nozzle diameter of breathing

	Nozzle diameter
velocity (m/s)	10
mass (kg)	0.0000077
dt_breath (s)	0.12
rho (kg/m3)	1019.32
d=	=ROT((C4*4)/(C6*C3*C5*3.14))

Figure 49: Nozzle diameter of cough

	Nozzle diameter
velocity (m/s)	4
mass (kg)	0.00000157
dt_breath (s)	8.4
rho (kg/m3)	1019
d=	=ROT((C4*4)/(C6*C3*C5*3.14))

Figure 50: Nozzle diameter of speech

B   Injector inputs

Injection temporal type:	SEQUENTIAL
Cyclic period:	5.0 s
Start of injection:	7.51 s ☐ Use file
Injection duration:	0.12 s ☐ Use file
Total injected mass:	7.7e-06 kg ☐ Use file
Total number of injected parcels (per nozzle):	3500
Injection drop distribution: ◉ Predefined ○ User-defined	Rosin-Rammler (based on SMD)
Rosin-Rammler parameter:	8.0

Figure 51: Inputs for cough sequence

Figure 52: Inputs for breathing sequence

Figure 53: Inputs for speaking sequence

C Model from Sketchup 2022
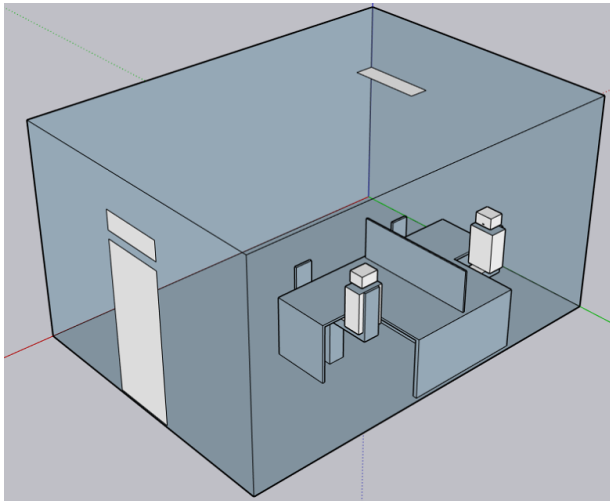
Figure 54: Mixing ventilation
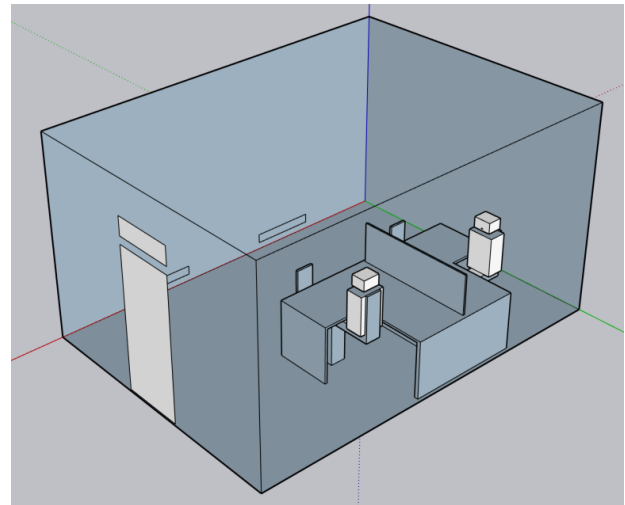
Figure 55: Displacement ventilation

D   Backflow
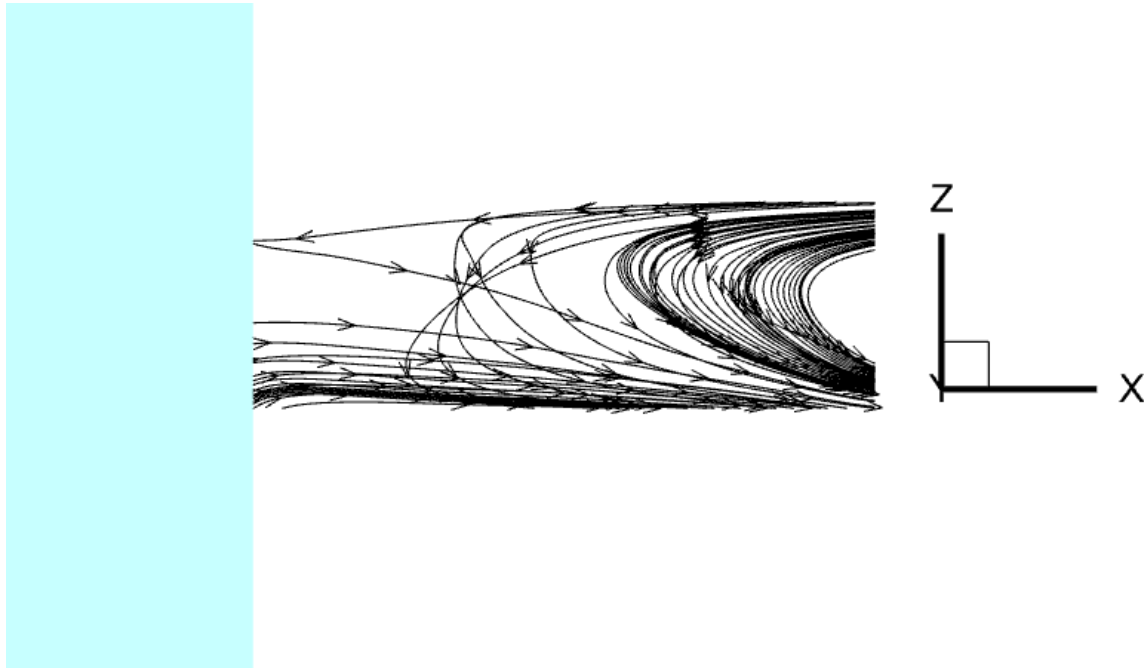
Figure 56: Backflow in outlet duct

E   Relative Humidity

Figure 57: Equations for RH in Tecplot

	P	Q	R	S	T	U
3	Room temperature		T_room [°C]	22		
4	Relative humidity room		RH_room [%]	50.0		
5	Molar mass H2O		Mm_H2O [g/mol]	18.01528		
6	Molar mass air		Mm_air [g/mol]	28.96470		
7	Saturated vapor pressure		P_sat [kPa]	2.644203		=0.61121*EKSP((18.678-(T3/234.5))*((T3/(257.14+T3))))
8	Vapor pressure		P_H2O [kPa]	1.322102		=(T4*T7/100)
9	Mole fraction vapor		Y_H2O	0.013048		=T8/101.325
10	Mole fraction air		Y_air	0.986952		=1-T9
11	Mass fraction H2O		ω_H2O	**0.008116**		=T9*(T5/T6)
12	Mass fraction O2		ω_O2	**0.231109**		=(1-T11)*0.233
13	Mass fraction N2		ω_N2	**0.760775**		=(1-T11)*0.767
14	SUM FRACTIONS			1.0		

Figure 58: Calculations of relative humidity

F Calculations for κ and ϵ

A_disp (m2)	0.64	one inlet
A_mixing (m2)	0.4	
Rho (kg/m3)	1.1861742	
v_mix (m/s)	0.0743	
v_disp (m/s)	0.0225	
dH_mix (m)	=(2*Y3)/(0.36+1.1)	
dH_disp (m)	=(2*Y2)/(0.44+1.45)	
dyn. Visc (N*s/m^2)	0.000018271517	
Re_mix	=(Y4*Y5*Y7)/Y9	
Re_disp	=(Y4*Y6*Y8)/Y9	
T_i_mix	=0.16*Y10^(-1/8)	
T_i_disp	=0.16*Y11^(-1/8)	
U'_mix	=ROT(1/3 * Y5^2)	
U'_disp	=ROT(1/3 * Y6^2)	

	TKE	Epsilon	Length scale
Mixing inlet	=2/3*(Y14*Y12^2)	=0.09^(3/4)*(Y17^(3/2)/AA17)	=0.07*Y7
Displacement inlet	=2/3*(Y15*Y13)^2	=0.09^(3/4)*(Y18^(3/2)/AA18)	=0.07*Y8

$$k = \frac{2}{3}(U_{ref}T_i)^2 \quad \varepsilon = C_\mu^{3/4}\frac{k^{3/2}}{\ell} \quad \ell = 0.07L$$

Figure 59: Calculations of tke and eps

G   Velocity profile for the mouth boundary, scenario 1

Table 4: Velocity profile, scenario 1, person 1 (speak and breathe)

Seconds	u	v	w
0	0	0	0
2.5	2.5	0	0
2.51	2.51	0	0
5	5	0	0
5.01	5.01	0	0
7.5	7.5	0	0
7.51	7.51	0	0
10	10	0	0
10.01	10.01	0	0
10.2	10.2	0	0
10.4	10.4	0	0
10.6	10.6	0	0
10.8	10.8	0	0
11	11	0	0
11.2	11.2	0	0
11.4	11.4	0	0
11.6	11.6	0	0
11.8	11.8	0	0
12	12	0	0
12.2	12.2	0	0
12.4	12.4	0	0
12.6	12.6	0	0
12.8	12.8	0	0
12.81	12.81	0	0
13.2	13.2	0	0
13.4	13.4	0	0
13.6	13.6	0	0
13.8	13.8	0	0
13.81	13.81	0	0
14.2	14.2	0	0
14.4	14.4	0	0
14.6	14.6	0	0
14.8	14.8	0	0
15	15	0	0
15.2	15.2	0	0
15.4	15.4	0	0
15.6	15.6	0	0
15.8	15.8	0	0
16	16	0	0
16.2	16.2	0	0
16.4	16.4	0	0
16.6	16.6	0	0
16.8	16.8	0	0
16.81	16.81	0	0
17.2	17.2	0	0
17.4	17.4	0	0
17.6	17.6	0	0
17.8	17.8	0	0
17.81	17.81	0	0
18.2	18.2	0	0
18.4	18.4	0	0
18.6	18.6	0	0
18.8	18.8	0	0
19	19	0	0
19.2	19.2	0	0
19.4	19.4	0	0
19.6	19.6	0	0
19.8	19.8	0	0
20	20	0	0
20.01	20.01	0	0
22.5	22.5	0	0
22.51	22.51	0	0
25	25	0	0
25.01	25.01	0	0
27.5	27.5	0	0
27.51	27.51	0	0
30	30	0	0
30.01	30.01	0	0
30.01	30.01	0	0

Table 5: Velocity profile, scenario 1, person 2 (cough and breathe)

Seconds	u	v	w
0	0	1	0
2.5	0	1	0
2.51	0	-1	0
5	0	-1	0
5.01	0	1	0
7.5	0	1	0
7.51	0	-1	0
10	0	-1	0
10.01	0	-10	0
10.13	0	-10	0
10.14	0	1	0
12.5	0	1	0
12.51	0	-1	0
15	0	-1	0
15.01	0	1	0
17.5	0	1	0
17.51	0	-1	0
20	0	-1	0
20.01	0	1	0
22.5	0	1	0
22.51	0	-1	0
25	0	-1	0
25.01	0	1	0
27.5	0	1	0
27.51	0	-1	0
30	0	-1	0
30.01	0	0	0

G.1 Velocity profile for mouth boundary, scenario 2

Table 6: Velocity profile, scenario 2, person 1 (speak and breathe)

Seconds	u	v	w
0	1	0	0
2.5	1	0	0
2.51	-1	0	0
5	-1	0	0
5.01	1	0	0
7.5	1	0	0
7.51	-1	0	0
10	-1	0	0
10.01	3.5	0	0
10.2	3.5	0	0
10.4	3.7	0	0
10.6	3.9	0	0
10.8	4	0	0
11	3.9	0	0
11.2	3.8	0	0
11.4	3.8	0	0
11.6	3.9	0	0
11.8	4	0	0
12	4	0	0
12.2	3.9	0	0
12.4	3.8	0	0
12.6	3.7	0	0
12.8	3.4	0	0
12.81	-1	0	0
13.01	-1	0	0
13.4	-1	0	0
13.6	-1	0	0
13.8	-1	0	0
13.81	3.9	0	0
14.2	4.1	0	0
14.4	4.1	0	0
14.6	4.5	0	0
14.8	4.5	0	0
15	4.2	0	0
15.2	4.2	0	0
15.4	3.9	0	0
15.6	3.8	0	0
15.8	3.9	0	0
16	3.9	0	0
16.2	4.1	0	0
16.4	4.1	0	0
16.6	3.9	0	0
16.8	3.9	0	0
16.81	-1	0	0
17.2	-1	0	0
17.4	-1	0	0
17.6	-1	0	0
17.8	-1	0	0
17.81	4.1	0	0
18.2	4.3	0	0
18.4	3.8	0	0
18.6	3.7	0	0
18.8	3.5	0	0
19	3.5	0	0
19.2	4.6	0	0
19.4	4.6	0	0
19.6	4.8	0	0
19.8	4.1	0	0
20	3.9	0	0
20.01	-1	0	0
22.5	-1	0	0
22.51	1	0	0
25	1	0	0
25.01	-1	0	0
27.5	-1	0	0
27.51	1	0	0
30	1	0	0
30.01	0	0	0

Table 7: Velocity profile, scenario 2, person 2 (cough and breathe)

Seconds	u	v	w
0	0	1	0
2.5	0	1	0
2.51	0	-1	0
5	0	-1	0
5.01	0	1	0
7.5	0	1	0
7.51	0	-1	0
10	0	-1	0
10.01	0	-10	0
10.13	0	-10	0
10.14	0	1	0
12.5	0	1	0
12.51	0	-1	0
15	0	-1	0
15.01	0	1	0
17.5	0	1	0
17.51	0	-1	0
20	0	-1	0
20.01	0	1	0
22.5	0	1	0
22.51	0	-1	0
25	0	-1	0
25.01	0	1	0
27.5	0	1	0
27.51	0	-1	0
30	0	-1	0
30.01	0	0	0

Table 8: Velocity profile, scenario 2, person 3 (speak and breathe)

Seconds	u	v	w
0	1	0	0
2.5	1	0	0
2.51	-1	0	0
5	-1	0	0
5.01	1	0	0
7.5	1	0	0
7.51	-1	0	0
10	-1	0	0
10.01	1	0	0
12.5	1	0	0
12.51	-1	0	0
15	-1	0	0
15.01	1	0	0
17.5	1	0	0
17.51	-1	0	0
19.99	-1	0	0
20	3.5	0	0
20.2	3.5	0	0
20.4	3.7	0	0
20.6	3.9	0	0
20.8	4	0	0
21	3.9	0	0
21.2	3.8	0	0
21.4	3.8	0	0
21.6	3.9	0	0
21.8	4	0	0
22	4	0	0
22.2	3.9	0	0
22.4	3.8	0	0
22.6	3.7	0	0
22.8	3.4	0	0
23	-1	0	0
23.2	-1	0	0
23.4	-1	0	0
23.6	-1	0	0
23.8	-1	0	0
24	3.9	0	0
24.2	4.1	0	0
24.4	4.1	0	0
24.6	4.5	0	0
24.8	4.5	0	0
25	4.2	0	0
25.2	4.2	0	0
25.4	3.9	0	0
25.6	3.8	0	0
25.8	3.9	0	0
26	3.9	0	0
26.2	4.1	0	0
26.4	4.1	0	0
26.6	3.9	0	0
26.8	3.9	0	0
27	-1	0	0
27.2	-1	0	0
27.4	-1	0	0
27.6	-1	0	0
27.8	-1	0	0
28	4.1	0	0
28.2	4.3	0	0
28.4	3.8	0	0
28.6	3.7	0	0
28.8	3.5	0	0
29	3.5	0	0
29.2	4.6	0	0
29.4	4.6	0	0
29.6	4.8	0	0
29.8	4.1	0	0
30	3.9	0	0
		0	0

H   Nozzle cone angle configuration for speech

Table 9: Profile configuration of nozzle cone angle

Seconds	Nozzle cone angle
0	30
0.2	35
0.4	40
0.6	30
0.8	45
1	30
1.2	40
1.4	30
1.6	35
1.8	30
2	40
2.2	45
2.4	30
2.6	40
2.8	40
3	40
3.2	30
3.4	30
3.6	35
3.8	35
4	35
4.2	30
4.4	40
4.6	40
4.8	45
5	45
5.2	35
5.4	35
5.6	35
5.8	35
6	40
6.2	35
6.4	40
6.6	35
6.8	40
7	35
7.2	35
7.4	35
7.6	35
7.8	30
8	30
8.2	30
8.4	40
8.6	40
8.8	40
9	30
9.2	30
9.4	30
9.6	35
9.8	35
10	35
11	0

I Sbatch file example

```
#!/bin/bash
# Job name:
#SBATCH --export=RLM_LICENSE=2765@SERVER_IP_ADDRESS
#SBATCH --job-name=cvg_boxman
#SBATCH --mem=100G
#
# Project:
#SBATCH --account=nn8005k
#
# Wall clock limit:
#SBATCH --mail-user=S326352@oslomet.no
#SBATCH --mail-type=END
#SBATCH --partition=bigmem

# Number of tasks (cores):

#SBATCH --nodes=3 --ntasks-per-node=32

# Max memory usage per task:
#####SBATCH --mem-per-cpu=3936
####SBATCH --mem-per-cpu=4G

#SBATCH --time=00:29:00

## Set up job environment:
####source /cluster/bin/jobsetup


set -o errexit # exit on errors
set -o nounset # Treat unset variables as errors
module --force purge

module use  /cluster/projects/nn8005k/CVG/V30/Convergent_Science/Environment/modulefiles/CONVERGE
module load CONVERGE-IntelMPI/3.0.24


## Set up input and output files:
tar -cvf temp.tar Boxman_normal/
mv temp.tar $SCRATCH

cd $SCRATCH
tar -xvf temp.tar
cd Boxman_normal/


mpirun converge-intelmpi super



rsync -arv  $SCRATCH/Boxman_normal  /cluster/projects/nn8005k/Ole/

exit 0
```

Figure 60: sbatch file example

J   Calculations of air flow

Displacement	V_p (m3/t)	Persons	V_mat (m3/h)	Area (m2)	Tot (m3/h)	Vel_inlet	ACH (SI-unit)
			Ventilation rates				
Norwegian recommendations	26	2	2.5	22	107	=P5/(3600*P2)	=(P5)/(5.5*4*3)
					214	=P6/(3600*P2)	=(P6)/(5.5*4*3)

Mixing	V_p (m3/t)	Persons	V_mat (m3/h)	Area (m2)	Tot (m3/h)		ACH (SI-unit)
Norwegian recommendations	26	2	2.5	22	107	=P9/(3600*P1)	=P9/(5.5*4*3)
					214	=P10/(3600*0.4)	=P10/(5.5*4*3)

Figure 61: Calculations of air flow